




This item was submitted to Loughborough's Institutional Repository (<https://dspace.lboro.ac.uk/>) by the author and is made available under the following Creative Commons Licence conditions.


 **creative commons**
C O M M O N S D E E D


Attribution-NonCommercial-NoDerivs 2.5


You are free:

- to copy, distribute, display, and perform the work

Under the following conditions:

 **Attribution.** You must attribute the work in the manner specified by the author or licensor.

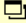
 **Noncommercial.** You may not use this work for commercial purposes.

 **No Derivative Works.** You may not alter, transform, or build upon this work.

- For any reuse or distribution, you must make clear to others the license terms of this work.
- Any of these conditions can be waived if you get permission from the copyright holder.

Your fair use and other rights are in no way affected by the above.

This is a human-readable summary of the [Legal Code \(the full license\)](#).

[Disclaimer](#) 

For the full text of this licence, please go to:
<http://creativecommons.org/licenses/by-nc-nd/2.5/>

1 **Synthesis and structural characterisation of new ettringite and thaumasite**

2 **type phases: $\text{Ca}_6[\text{Ga}(\text{OH})_6 \cdot 12\text{H}_2\text{O}]_2(\text{SO}_4)_3 \cdot 2\text{H}_2\text{O}$ and**

3 **$\text{Ca}_6[\text{M}(\text{OH})_6 \cdot 12\text{H}_2\text{O}]_2(\text{SO}_4)_2(\text{CO}_3)_2$, $\text{M}=\text{Mn}, \text{Sn}$**

4 Rachel L. Norman,^{a,b} Sandra E. Dann^a, Simon C. Hogg^c and Caroline A. Kirk^{*a,b}

5 ^aDepartment of Chemistry, Loughborough University, Loughborough, LE11 3TU, U.K.

6 ^bDepartment of Mineralogy, The Natural History Museum, Cromwell Road, London,
7 SW7 5BD, U.K.

8 ^cDepartment of Materials, Loughborough University, Loughborough, LE11 3TU, U.K.

9 * corresponding author, C.A.Kirk@lboro.ac.uk

10

11

12 **Abstract**

13

14

15 Investigations into the formation of new ettringite-type phases with a range of

16 trivalent and tetravalent cations were carried out to further study the potential this

17 structure type has to incorporate cations covering a range of ionic radii (0.53-0.69 Å).

18 We report the synthesis and structural characterisation of a new ettringite-type phase,

19 $\text{Ca}_6[\text{Ga}(\text{OH})_6 \cdot 12\text{H}_2\text{O}]_2(\text{SO}_4)_3 \cdot 2\text{H}_2\text{O}$, which was indexed in space group P31c with the

20 unit cell parameters $a = 11.202(2)$ Å, $c = 21.797(3)$ Å and two new thaumasite-type

21 phases $\text{Ca}_6[\text{M}(\text{OH})_6 \cdot 12\text{H}_2\text{O}]_2(\text{SO}_4)_2(\text{CO}_3)_2$, $\text{M} = \text{Mn}, \text{Sn}$ which were indexed in space

22 group $P6_3$ with the unit cell parameters $a = 11.071(5) \text{ \AA}$, $c = 21.156(8) \text{ \AA}$ and $a =$
23 $11.066(1) \text{ \AA}$, $c = 22.420(1) \text{ \AA}$ respectively. These new phases show the versatility of
24 the ettringite family of structures to tolerate a large range of cation sizes on the
25 octahedral M site and highlights the preference of tetravalent cations to crystallise
26 with the thaumasite structure over the ettringite structure.

27

28

29 *Keywords:* Ettringite; Thaumasite; X-ray Diffraction, Synchrotron.

30

31 **1. Introduction**

32

33

34 Ettringite, $\text{Ca}_6[\text{Al}(\text{OH})_6 \cdot 12\text{H}_2\text{O}]_2(\text{SO}_4)_3 \cdot 2(\text{H}_2\text{O})$ and thaumasite,
35 $\text{Ca}_3[\text{Si}(\text{OH})_6 \cdot 12\text{H}_2\text{O}](\text{SO}_4)(\text{CO}_3)$, are minerals that occur as secondary alteration
36 phases in mafic, igneous and metamorphic rocks [1,2]. They also form in cement
37 pastes, mortars and concretes, in field structures and when made in the laboratory.
38 Ettringite forms as a hydration product of tricalcium aluminate in the presence of
39 sulphate ions in Portland cements. Thaumasite forms in ordinary and sulphate-
40 resisting Portland cements, when stored at low temperatures, in damp conditions, in
41 the presence of carbonate ions and an external supply of sulphate ions [3]. However,
42 there is one report of thaumasite forming in Portland cements in warm climates [4].

43

44 The chemistry of ettringite can be altered to produce thaumasite through
45 replacement of aluminium with silicon as well as replacing one of the sulphate
46 groups and two molecules of water with two carbonate groups. This allows for the
47 more positively charged Si^{4+} replacing Al^{3+} [3]. Thaumasite and ettringite are also
48 structurally related; both adopt hexagonal structures, but with different space groups.
49 Ettringite crystallises in space group $P31c$ with $a = 11.224 \text{ \AA}$, $c = 21.108 \text{ \AA}$ [5,6] and
50 thaumasite crystallises in space group $P6_3$ with $a = 11.04 \text{ \AA}$, $c = 10.39 \text{ \AA}$. [7,8] Solid
51 solutions exist between these two phases, however, there are reported
52 discontinuities in the unit cell parameters attributed to the different space groups
53 each of the phases crystallise in [9].

54

55 The structures of ettringite and thaumasite can be described as consisting of cation
56 and anion columns. Ettringite consists of cation columns with composition
57 $\text{Ca}_3[\text{Al}(\text{OH})_6 \cdot 12\text{H}_2\text{O}]^{3+}$, that run parallel to the c axis, with the sulphate anions and
58 remaining water molecules in channels running parallel to these columns (Fig. 1).
59 Thaumasite has a cylindrical column of composition $\text{Ca}_3[\text{Si}(\text{OH})_6 \cdot 12\text{H}_2\text{O}]^{3+}$ that runs
60 parallel to the c axis, with the sulphate and carbonate anions ordered in the channels
61 between the columns, which also contain water molecules [3,7]. Thaumasite is
62 especially unusual as the tetravalent silicon ion is octahedrally co-ordinated by (OH^-)
63 [1]; only one other phase is known, $\text{Si}_2\text{P}_2\text{O}_7$, that can form at ambient pressures with
64 Si^{4+} octahedrally co-ordinated [10].

65

66 Ettringite has been shown to accommodate a wide range of both cations and anions
67 [11-13]. Mineral samples of ettringite can contain trace amounts of Fe^{3+} and Si^{4+} ,

68 substituting for the Al^{3+} on the octahedral site [14]. The existence of minerals which
69 contain significant amounts of Fe^{3+} or Si^{4+} are distinct, but related, mineral species,
70 known as sturmanite, $\text{Ca}_6[(\text{Fe}_{0.6}\text{Al}_{0.2}\text{Mn}_{0.2})(\text{OH})_6 \cdot 12\text{H}_2\text{O}]_2(\text{SO}_4)_{2.7}[\text{B}(\text{OH})_3]_{0.3}[\text{B}(\text{OH})_4]$
71 and charlesite, $\text{Ca}_6[(\text{Al},\text{Si})(\text{OH})_6 \cdot 12\text{H}_2\text{O}]_2(\text{SO}_4)_2[\text{B}(\text{OH})_4]_2 \cdot \text{H}_2\text{O}$ [15,16]. They also
72 exhibit substitution of some of the sulphate groups with borate polyanions.

73

74 There are two reported thaumasite-type minerals, jouravskite
75 $\text{Ca}_3[\text{Mn}(\text{OH})_6 \cdot 12\text{H}_2\text{O}](\text{SO}_4)(\text{CO}_3)$ [17] and carraraite $\text{Ca}_3[\text{Ge}(\text{OH})_6 \cdot 12\text{H}_2\text{O}](\text{SO}_4)(\text{CO}_3)$
76 [18], which have the octahedral site, occupied by Si^{4+} in thaumasite, replaced by the
77 tetravalent cations Mn^{4+} and Ge^{4+} .

78

79 Synthetic studies to date have focused mainly on sulphate anion replacement in
80 ettringite, with reports of ettringite-type phases forming with many anions, e.g. NO_3^- ,
81 $\text{B}(\text{OH})_4^-$, OH^- , SO_3^{2-} , CrO_4^{2-} , CO_3^{2-} , Cl^- [11,12]. Investigations into the solid solution
82 formation between ettringite and its carbonate analogue have been carried out [19].

83 The lattice parameter trends indicate the two end members form partial solid
84 solutions and there is no continuous solid solution between the end members.

85 These results are similar to the discontinuities in the lattice parameters found
86 between ettringite and thaumasite end members [3,9].

87

88 Our investigations here have focused on substitution of the Al^{3+} site by trivalent and
89 tetravalent cations. We have successfully synthesised one new ettringite-type phase,
90 $\text{Ca}_6[\text{Ga}(\text{OH})_6 \cdot 12\text{H}_2\text{O}](\text{SO}_4)_3 \cdot 2(\text{H}_2\text{O})$ and two new thaumasite-type phases,

91 $\text{Ca}_6[\text{M}(\text{OH})_6 \cdot 12\text{H}_2\text{O}](\text{SO}_4)_2(\text{CO}_3)_2$, M=Mn and Sn. During this study, ettringite, and
92 the reported iron analogue, $\text{Ca}_6[\text{Fe}(\text{OH})_6 \cdot 12\text{H}_2\text{O}](\text{SO}_4)_3 \cdot 2\text{H}_2\text{O}$ [20,21] were also
93 synthesised under the same conditions. Here we report the characterisation of the
94 ettringite and thaumasite type phases using both in-house techniques (powder X-ray
95 Diffraction and infrared spectroscopy) as well as high resolution synchrotron powder
96 X-Ray Diffraction, on beamline I11 at The Diamond Light Source.

97

98 **2. Experimental**

99

100

101 The ettringite-type phases were prepared using a variation on the saccharate
102 method, [21] whereby a solution of $\text{M}_2(\text{SO}_4)_3$, M= Al^{3+} , Fe^{3+} , Ga^{3+} or MSO_4 , M= Mn^{2+} ,
103 Sn^{2+} (Sigma-Aldrich 99.9% pure), was added to a solution of CaO (Sigma-Aldrich
104 99.9% pure) in a 6:1 (Ca:M) ratio. The CaO was heated overnight at 1000 °C, to
105 ensure the removal of water and decarbonation of any calcium carbonate, then
106 dissolved in a 10 % sugar solution (10 g of sugar in 100 ml distilled water) and mixed
107 using a magnetic stirrer. In a second beaker, the appropriate metal sulphate was
108 dissolved in 100 ml of distilled water and then added to the CaO solution. The
109 beaker was covered with parafilm and left on a stirrer plate at room temperature
110 overnight. After 24 h the solution was vacuum filtered and left in a desiccator to dry.
111 The precipitates were analysed by powder X-ray Diffraction (PXRD) and infrared
112 spectroscopy (IR).

113

114 PXRD data were collected on a Bruker D8 Advance diffractometer in reflection
115 geometry, Cu K α_1 radiation and a Braun linear position sensitive detector. Data were
116 collected over the 2θ range 5-90° with a step size of 0.007° 2θ and a count time of
117 1.8 s per step. NIST SRM640c silicon was added as an internal standard. Lattice
118 parameters were determined using a least squares refinement procedure, part of the
119 Stoe WinXPow software suite. IR spectra were collected on neat powders using a
120 Shimadzu FTIR 8400S Spectrophotometer with a Specac Golden Gate attachment
121 between 400-4000 cm⁻¹.

122

123 Synchrotron Radiation PXRD data were collected at room temperature on the
124 ettringite and thaumasite type phases at The Diamond Light Source (Didcot, UK), I11
125 beamline, High Resolution Powder Diffractometer [23]. The samples were mounted
126 in 0.5 mm Lindemann capillaries and measured in Debye-Scherrer (transmission)
127 geometry. The data were collected over the 2θ range 5°-150° 2θ for 30 minutes.
128 The X-ray wavelength (0.826262 Å) and 2θ zero offset were calibrated by refinement
129 of the diffraction pattern of a silicon standard (NIST SRM640c). Data were refined
130 using the refinement package Topas Academic v4 [24]. Rietveld refinement was
131 carried out for each dataset to investigate whether the samples crystallised with
132 either the ettringite or thaumasite type structure.

133

134

135

136 **3. Results**

137

138

139 **3.1 X-ray Diffraction**

140

141 Fig. 2 shows the laboratory PXRD patterns of the phases formed from the above
142 synthetic procedure. Comparison to the International Center for Diffraction Data
143 Powder Diffraction File (ICDD PDF) confirmed the phases to be ettringite type (ICDD
144 No 41-1451) [5]. Synthesis of ettringite under the same experimental conditions was
145 carried out and is included on Fig. 2 for comparison purposes. Many synthetic
146 studies of the formation of ettringite are carried out under CO₂-free conditions due to
147 the reported formation of CaCO₃ [9,11,12]. Analysis of the PXRD data showed that
148 only the Fe ettringite-type phase had a trace amount of CaCO₃ present, whereas all
149 other samples were found to contain only ettringite-type crystalline phases (within
150 the detection limits of the PXRD technique). This suggests that the addition of CaO
151 to a sucrose solution, to improve the solubility of CaO had also reduced and in some
152 cases prevented, the formation of CaCO₃. It should be noted that the broad
153 background feature around 10° 2θ may be due to the presence of amorphous gel-
154 like phases that often form as pre-cursors in synthetic cement-type systems [25].
155 Results of the lattice parameter refinements carried out on the laboratory PXRD data,
156 are shown in Table 1.

157

158

159 **3.2 Infrared Spectroscopy**

160

161 IR data were also used to confirm the phases present were ettringite type and to
162 investigate the presence of functional groups in the structures. Comparison of the IR
163 spectra of the new phases to the IR spectrum of pure ettringite shows similarities
164 suggesting the phases formed are ettringite (Fig. 3). The broad band at 3400 cm^{-1} is
165 indicative of the water vibrations in the channel of the structure (Fig.1), the stretch in
166 the region 1100 cm^{-1} is characteristic of the presence of sulphate groups and the
167 band in the region 1400 cm^{-1} would indicate the presence of the CO_3^{2-} group [26,27].
168 The IR spectrum of CaCO_3 is included for comparison.

169

170 **3.3 Rietveld refinement of synchrotron PXRD data**

171

172 Initial analysis of the high resolution PXRD data collected on beamline I11 showed
173 that the Al and Fe substituted ettringite samples and the thaumasite-type samples
174 contained impurity phases, not detected on analysis of the laboratory PXRD data.
175 Table 2 gives details of the phases identified to be present in each sample.

176

177 Refinement strategy

178

179 Full structural refinements were carried out using the Rietveld refinement method in
180 the refinement programme Topas Academic [24]. The initial strategy used for each
181 refinement was the same, whereby the background was modelled using a

182 Chebychev function and the peak shape modelled using the modified Thomson-Cox-
183 Hasting pseudo Voigt function with the asymmetry of low angle peaks modelled
184 using a simple axial model.

185

186 The ettringite-type phases $\text{Ca}_6[\text{M}(\text{OH})_6 \cdot 12\text{H}_2\text{O}]_2(\text{SO}_4)_3 \cdot 2\text{H}_2\text{O}$, $\text{M}=\text{Al}, \text{Fe}, \text{Ga}$ were
187 refined using a published ettringite structural model as a starting point, with the
188 occupancy of the O19 site, the oxygen atom of the unbound water molecule in the
189 anion column (Fig. 1b), fixed at 2/3 as in the published model [6]. After refinement of
190 the background, lattice parameters and profile parameters had converged the
191 thermal parameters (beq) were then refined. Although it is more normal to refine the
192 atomic positions before the thermal parameters, after testing many different
193 strategies, this chosen one was found to produce the most stable refinements. The
194 thermal parameters of the O sites were then constrained in sets to give stable
195 refinements; O1-O4 (O sites co-ordinated to the M cation), O5-O12 (O sites co-
196 ordinated to just the Ca sites) and O13-O18, (O sites co-ordinated to the S sites),
197 and the thermal parameters of the S sites were also constrained. The atomic
198 positions were then refined and finally all variable parameters were allowed to refine
199 until the least squares refinement converged. In the case of the Ga sample, all
200 constraints on the thermal parameters could be removed, but for the Al and Fe
201 samples this was not possible. The sulphate anions in both the Al and Fe
202 substituted samples were especially problematic to refine and give reasonable
203 calculated S-O bond lengths and beq. Therefore the positional parameters were
204 fixed to those of the structural model [6].

205

206 Refinement of the thaumasite phases, $\text{Ca}_6[\text{M}(\text{OH})_6 \cdot 12\text{H}_2\text{O}]_2(\text{SO}_4)_2(\text{CO}_3)_2$, $\text{M} = \text{Mn}$,
207 Sn , were carried out using a published structural model as a starting point [8]. The
208 initial refinement strategy was the same as for the ettringite phases and constraints
209 were placed on the O thermal parameters. In general, for both thaumasite phases, a
210 stable refinement of the carbonate and sulphate anions was not achieved and in
211 both cases, the C and S thermal parameters were fixed at 1. More reasonable C-O
212 and S-O bond lengths were produced using this strategy.

213

214 Refinement of $\text{Ca}_6[\text{Al}(\text{OH})_6 \cdot 12\text{H}_2\text{O}]_2(\text{SO}_4)_3 \cdot 2\text{H}_2\text{O}$

215 The ettringite sample, $\text{Ca}_6[\text{Al}(\text{OH})_6 \cdot 12\text{H}_2\text{O}]_2(\text{SO}_4)_3 \cdot 2\text{H}_2\text{O}$ was found to be multiphase,
216 (Table 2), therefore a multiphase Rietveld refinement was carried out. The final
217 observed-calculated and difference profiles (Fig. ESI 1) and the refined atomic
218 positions and thermal parameters (Table ESI 1) are provided as electronic
219 supplementary information and the calculated bond lengths are shown in Table 3.

220

221 Refinement of $\text{Ca}_6[\text{Fe}(\text{OH})_6 \cdot 12\text{H}_2\text{O}]_2(\text{SO}_4)_3 \cdot 2\text{H}_2\text{O}$

222 The Fe substituted ettringite phase $\text{Ca}_6[\text{Fe}(\text{OH})_6 \cdot 12\text{H}_2\text{O}]_2(\text{SO}_4)_3 \cdot 2\text{H}_2\text{O}$ was also
223 found to have impurity phases present (Table 2) and therefore a multiphase Rietveld
224 refinement of these data was carried out. To allow a stable refinement, the
225 constraints on the thermal parameters, as indicated in the refinement strategy, were
226 introduced as well as fixing the atomic co-ordinates of the position O19. The final
227 observed, calculated and difference profile (Fig. ESI 2) and the refined atomic

228 positions and thermal parameters (Table ESI 2) are provided as electronic
229 supplementary information and the calculated bond lengths are given in Table 3.

230

231

232 Refinement of $\text{Ca}_6[\text{Ga}(\text{OH})_6 \cdot 12\text{H}_2\text{O}]_2(\text{SO}_4)_3 \cdot 2\text{H}_2\text{O}$

233 The Ga substituted ettringite phase, $\text{Ca}_6[\text{Ga}(\text{OH})_6 \cdot 12\text{H}_2\text{O}]_2(\text{SO}_4)_3 \cdot 2\text{H}_2\text{O}$ was found to
234 be phase pure and refinement of this dataset produced a very stable refinement,
235 whereby all parameters could be refined and no constraints were required. The final
236 observed, calculated and difference plots (Figure ESI 3) and the refined atomic
237 positions and thermal parameters (Table ESI 3) are provided as electronic
238 supplementary information and the calculated bond lengths are presented in Table 3.

239

240 Refinement of $\text{Ca}_6[\text{M}(\text{OH})_6 \cdot 12\text{H}_2\text{O}]_2(\text{SO}_4)_2(\text{CO}_3)_2$, M=Mn, Sn

241 The Sn and Mn compounds had the targeted compositions

242 $\text{Ca}_6[\text{M}(\text{OH})_6 \cdot 12\text{H}_2\text{O}]_2(\text{SO}_4)_3 \cdot 2\text{H}_2\text{O}$, M = Mn, Sn. However, both were determined to
243 contain carbonate units as shown by IR (Fig. 3, band at $\sim 1400 \text{ cm}^{-1}$) and the PXRD
244 data could be refined on a smaller unit cell, related to that of thaumasite (Table 1).

245 The composition is therefore proposed to be similar to that of thaumasite

246 $\text{Ca}_6[\text{M}(\text{OH})_6 \cdot 12\text{H}_2\text{O}]_2(\text{SO}_4)_2(\text{CO}_3)_2$, M=Mn, Sn. The Sn and Mn thaumasite-type
247 phases were shown to contain an impurity phase, that has yet to be identified and
248 therefore single phase Rietveld refinements were carried out. In both refinements it
249 was difficult to achieve a stable refinement of the sulphate and carbonate anions and
250 constraints on the O sites were introduced, which included fixing the thermal

251 parameter of the O5 site at 1 during refinement of the Sn phase. The thermal
252 parameter of the C1 site was fixed at 1 during the refinement of both the thaumasite
253 phases and the thermal parameter of the S1 site was fixed at 1 during refinement of
254 the Sn phase. To produce a stable refinement of the Mn-thaumasite phase, the
255 atomic positions of the S1 and C1 sites were fixed at the values given in the starting
256 model [8].

257

258 The final observed, calculated and difference profiles for the Mn-substituted
259 thaumasite phase $\text{Ca}_6[\text{Mn}(\text{OH})_6 \cdot 12\text{H}_2\text{O}]_2(\text{SO}_4)_2(\text{CO}_3)_2$, (Fig. ESI 4) and the refined
260 atomic positions and thermal parameters (Table ESI 4) are provided as
261 supplementary electronic information and the calculated bond lengths are presented
262 in Table 4. The observed, calculated and difference profiles from refinement of the
263 data collected on the Sn-thaumasite phase $\text{Ca}_6[\text{Sn}(\text{OH})_6 \cdot 12\text{H}_2\text{O}]_2(\text{SO}_4)_2(\text{CO}_3)_2$, are
264 shown (Fig. ESI 5) and the refined atomic position and thermal parameters (Table
265 ESI 5) are presented as electronic supplementary information and the calculated
266 bond lengths are shown in Table 4.

267

268 Bond Valence Analysis

269 Using the calculated bond lengths for each of the ettringite and thaumasite phases,
270 bond valence analysis was carried out [28]. Table 5 presents the valences
271 determined for each of the cations in all of the investigated phases.

272

273

274

275 4. Discussion

276

277 Laboratory PXRD data, IR data and refinement of the synchrotron PXRD data
278 confirmed the compositions $\text{Ca}_6[\text{M}(\text{OH})_6 \cdot 12\text{H}_2\text{O}]_2(\text{SO}_4)_3 \cdot 2\text{H}_2\text{O}$, M=Al, Fe, Ga
279 crystallised with an ettringite-type structure. Only the Ga substituted compound was
280 found to be single phase whereas the Al and Fe substituted phases had impurities
281 present (Table 2). The IR spectrum of the Fe substituted phase has a strong band at
282 1415 cm^{-1} indicating the presence of a CO_3^{2-} ion (Fig. 3); this confirms the result from
283 analysis of the PXRD datasets (both laboratory and synchrotron) which show a trace
284 amount of CaCO_3 to be present. The other impurity phases identified on analysis of
285 the synchrotron PXRD data may be due to the degradation of the samples, given the
286 time period between synthesis of the samples and data collection on beamline I11 (2
287 months).

288

289 The Mn and Sn substituted compounds were synthesised under the same conditions
290 as the ettringite-type phases. The PXRD data when compared to the standard
291 ettringite pattern exhibited shifts in 2θ positions, as expected due to the different
292 ionic radii of the cations occupying the octahedral site. However, there were notable
293 missing key reflections associated with an ettringite-type diffraction pattern. Fig. 4
294 highlights an expanded range of PXRD data with the hkl indices marked on the
295 reflections for ettringite; the 002, 101, 103 and 104 are absent. This, along with
296 other absent reflections for an ettringite-type structure at higher 2θ values (not

297 shown here) suggested that the Mn and Sn phases were thaumasite-type structures.
298 The IR spectra for the Mn and Sn compounds clearly showed the presence of a
299 carbonate group at $\sim 1375\text{ cm}^{-1}$ (Fig. 3). Analysis of the PXRD data (both lab and
300 synchrotron) found no evidence for the presence of CaCO_3 in quantities detectable
301 by PXRD. As the syntheses were carried out in air, we propose that CO_2 from the
302 atmosphere has dissolved into the solutions during synthesis and suggest this is the
303 source of the carbonate ions. We therefore conclude the carbonate is likely to be
304 structurally incorporated in the Sn and Mn compounds, rather than present as a
305 separate impurity phase. Structural refinement of the synchrotron PXRD data using
306 a thaumasite model confirmed both the Sn and Mn substituted compounds
307 crystallise with a thaumasite-type structure.

308

309 The Mn-substituted phase is a synthetic analogue of the mineral jouravskite and the
310 oxidation state of the Mn in jouravskite is suggested to be 4+ [17]. We therefore
311 suggest the Mn in the synthetic jouravskite phase is also tetravalent. This study
312 suggests that when sources of Ca ions and sulphate anions are in the presence of
313 tetravalent metal cations, thaumasite rather than ettringite-type phases are formed
314 incorporating carbonate into the structure to balance the extra positive charge of the
315 octahedral cation (tetravalent versus trivalent in ettringite).

316

317 The refined unit cell parameters for all the ettringite and thaumasite type phases are
318 plotted against the ionic radii for the octahedral cations and presented in Fig. 5.
319 Included for comparison are the published lattice parameters for ettringite and
320 thaumasite [5,7]. The c parameters for all the thaumasite type-phases have been

321 doubled for comparison. This plot shows that as the ionic radii of the octahedral
322 cations increase, the *c* parameter also increases. The refined *a* unit cell parameter
323 shows two trends depending on whether the structure is ettringite or thaumasite-type.
324 The ettringite-type structures (M=Al, Ga, Fe) show a decrease in *a* as the ionic radii
325 increase. Whereas the refined *a* unit cell parameters for the thaumasite-type phases
326 are clustered and are shorter than those of the ettringite-type compounds. This is
327 further evidence that the Mn and Sn phases have a thaumasite-type structure and
328 fits well with previous work on thaumasite-ettringite solid solutions where the *a*
329 parameters of thaumasite members are in the range 11.054-11.11 Å [3,9].

330

331 Structural refinements of the synchrotron PXRD data were only possible through
332 introduction of constraints on the thermal parameters and, in some cases, the atomic
333 positions, as highlighted in the results section. Refinement of the ettringite sample
334 proved to be rather problematic, which was partly due to the data quality, as the
335 sample was found to be multiphase containing three crystalline impurity phases
336 (Table 2) and a suspected amorphous phase, present as a hump in the dataset
337 around 11° 2θ. Gypsum (CaSO₄.2H₂O) is a common degradation product of natural
338 ettringite minerals and this phase was found to be present in the sample. It is likely
339 the sample has degraded between being synthesised and data collection on I11 as
340 the impurity phases were not observed on analysis of the laboratory PXRD data.

341

342 Analysis of the bond lengths shows the Al-O and Ca-O to be within acceptable
343 ranges for such polyhedra, which is confirmed by the bond valence analysis (Table
344 5). The fixed sulphate units have good bond lengths, but the thermal parameters

345 refine to rather high values. This suggests there are issues with the sulphate anions
346 in this structure and it is thought to be due to disorder within the anion column.
347 Further analysis of low temperature data is required to resolve this.

348

349 Refinement of data collected on the Fe substituted sample also produced high
350 thermal parameters of the O atoms which bond to the sulphur atoms, again
351 indicating that there is possible disorder in the anion column. The other issue with
352 this refinement is the highly disordered nature of the Fe1 octahedra, with very short
353 Fe1-O2 bond lengths. Initially it was assumed the Fe³⁺ may be in the high spin state
354 introducing a Jahn-Teller distortion of the Fe1 octahedra; this was not replicated by
355 the Fe2 octahedra, which is much more regular. Again, further analysis of low
356 temperature synchrotron data is required to try and resolve these issues.

357

358 The Ga substituted sample was shown to be single phase and highly crystalline.
359 Refinement of the data collected on this sample was very stable and all constraints
360 could be lifted. The thermal parameters of certain O sites have large errors and this
361 is especially the case for the sulphate anions. Bond valence analysis shows that the
362 Ga and Ca valences are close to their ideal values, but the sulphur ions deviate a lot
363 from the expected 6+. The bond lengths between the S and O atoms of the sulphate
364 anions are somewhat longer than the reported bond lengths for ettringite, but the unit
365 cell is larger and again it is likely that the anion columns are highly disordered.

366

367 Refinement of the datasets collected on the thaumasite-type phases,
368 $\text{Ca}_6[\text{M}(\text{OH})_6 \cdot 12\text{H}_2\text{O}]_2(\text{SO}_4)_2(\text{CO}_3)_2$, $\text{M}=\text{Mn}, \text{Sn}$, were carried out using the constraints
369 as detailed in the results section. The Mn-substituted phase has calculated Mn-O
370 and Ca-O bond lengths that are acceptable, which is reinforced by the bond valence
371 analysis (Table 5). Refined parameters from the thaumasite composition
372 $\text{Ca}_6[\text{Sn}(\text{OH})_6 \cdot 12\text{H}_2\text{O}]_2(\text{SO}_4)_2(\text{CO}_3)_2$ gave calculated C-O bond lengths shorter than
373 those for carbonate in the thaumasite structure and the S-O bond lengths in the
374 basal plane of the sulphate anion are longer than those calculated from the atomic
375 positions for thaumasite as given by Jacobsen et al [8]. Bond valence analysis
376 carried out from the calculated bond lengths show that the carbon atom is slightly
377 over bonded, due the short bond length but the sulphur atom is very underbonded
378 due to these long bond lengths. It is suggested that the anion columns in the
379 thaumasite-type phases are also very disordered and refinement of low temperature
380 data may allow a more stable refinement.

381

382 Table 6 shows details of the range of cation bond lengths and average values
383 determined for each of the phases investigated here. The average cation-oxygen
384 bond lengths are plotted as a function of M cation radius and presented in Fig. 6.
385 The Ca-O bond lengths show very little change as a function of M cation radius,
386 whereas the M-O bond lengths increase as the M cation radius increases, the S-O
387 and C-O bond lengths show no obvious trend as a function of M cation radius.

388

389

390

391

392

393 **5. Conclusions**

394

395

396 Investigations into the formation of new substituted ettringite-type phases, replacing
397 the octahedral Al cation with other trivalent as well as tetravalent cations has been
398 carried out. We have successfully synthesised ettringite, Fe-substituted ettringite
399 and a new Ga-substituted ettringite using a simple precipitation method, whereby a
400 sucrose solution was used to improve the solubility of CaO and attempt to inhibit the
401 formation of CaCO₃. This method was only partially successful, reducing the amount
402 of calcite formed, in the case of ettringite and Fe-ettringite and inhibiting its formation
403 in the case of the Ga, Mn and Sn substituted phases. However, it is evident that
404 some CO₂ did dissolve into the solutions as, in the presence of tetravalent cations
405 (Mn⁴⁺ and Sn⁴⁺), the phases formed were thaumasite-type, which have CO₃²⁻ anions
406 structurally incorporated. . This was confirmed through the presence of a carbonate
407 stretch in the IR spectra, not observed for the ettringite-type phases. The
408 incorporation of carbonate into the structure allows for the more positively charged
409 tetravalent cations to replace Al³⁺ in the ettringite structure, whereby two carbonate
410 anions replace one sulphate anion and two water molecules. The PXRD data were
411 also indexed with a thaumasite-type unit cell.

412

413 Structural refinements of all the phases were carried out through refinement of high
414 resolution synchrotron powder XRD data. This confirmed that the compositions
415 $\text{Ca}_6[\text{M}(\text{OH})_6 \cdot 12\text{H}_2\text{O}]_2(\text{SO}_4)_3 \cdot 2\text{H}_2\text{O}$, M= Al, Fe and Ga crystallised with the ettringite
416 structure type and the compositions $\text{Ca}_6[\text{M}(\text{OH})_6 \cdot 12\text{H}_2\text{O}]_2(\text{SO}_4)_2(\text{CO}_3)_2$, M = Mn, Sn
417 crystallised with the thaumasite type structure.

418

419 Under laboratory conditions, the synthesis of thaumasite is a lengthy process and
420 requires low temperatures (0-5°C) [29]. However, the formation of the Mn and Sn
421 substituted thaumasite phases occurs at room temperature and within 24 hours. It is
422 likely that the Mn and Sn thaumasite phases form more readily than pure thaumasite
423 as these tetravalent cations have large ionic radii and adopt octahedral co-ordination
424 more readily than Si^{4+} , which is more commonly tetrahedrally co-ordinated under
425 ambient pressures.

426

427 As there are still issues with the phase purity of some of the samples and to confirm
428 the thaumasite-type phases will only form in the presence of CO_2 , synthesis of all the
429 targeted compositions under N_2 will be attempted. Also, to resolve the issues with
430 some of the structural refinements, low temperature synchrotron powder XRD data
431 has now been collected and refinement of these datasets will be used to test the
432 hypothesis that the anion columns are highly disordered.

433

434 **Acknowledgements**

435

436

437 CK would like to acknowledge preliminary work carried out on this project by
438 Stephen Cairns, with financial support from The Natural History Museum and
439 WestChem. She would also like to thank Prof Chui Tang and Dr Julia Parker,
440 beamline scientists on the I11 beamline at the Diamond Light Source, for their
441 assistance in setting up the beamline to carry out these experiments, Philip Davies,
442 for his initial work on analysis of the synchrotron data during his undergraduate
443 research project and Prof Chick Wilson, for his continued support on this project.

444

445

446 **References**

447

448

449 [1] D. McConnel and J. Murdoch, *Min. Mag.*, 33 (1962), pp. 59-64

450 [2] R.A. Edge, H.F.W Taylor, *Nature*, 224 (1969), pp363-364

451 [3] S.M. Torres, C.A. Kirk, C.J. Lynsdale, R.N. Swamy and J.H. Sharp, *Cem. Concr.*
452 *Res.*, 34 (2004), pp. 1297-1305

453 [4] S. Diamond, *Cem. Concr. Res.*, 25(8) (2003), pp. 1161-1164

454 [5] A.E. Moore and H.F.W. Taylor, *Acta Cryst.*, B26 (1970), pp. 386-393

455 [6] F. Goetz-Neunhoeffler and J. Neubauer, *Powder Diffraction*, 21 (2006), pp 4-11

456 [7] R.A. Edge and H.F.W. Taylor, *Acta Cryst.*, B27 (1971), pp. 594-601

- 457 [8] S.D. Jacobsen, J.R. Smythe and R.J. Swope, *Phys. Chem, Mineral.*, 30 (2003),
458 pp. 321-329
- 459 [9] S.J. Barnett, C.D. Adam and A.R.W. Jackson, *J. Mater. Sci.*, 35 (2000), pp. 4109-
460 4114
- 461 [10] E. Tillmanns, W. Gebert and W.H. Baur, *J. Solid State Chem.*, 7 (1973), pp. 69-
462 84
- 463 [11] H. Poellmann and H.J. Kuzel, *Cem. Concr. Res.*, *Cem. Conr. Res.*, 20 (1990),
464 pp. 941-947
- 465 [12] H. Poellmann and R. Wenda, *Cem. Concr. Res.*, 23 (1993), pp. 422-430
- 466 [13] M.L.D. Gougar, B.E. Scheetz and D.M. Roy, *Waste Manage.*, 16(4) (1996), pp.
467 295-303
- 468 [14] S. Cairns, C.C. Wilson and C.A. Kirk, Structural studies of ettringite-type
469 minerals in the collections of the Natural History Museum, London, unpublished
470 results
- 471 [15] D.Y. Puschcarovsky, Y.S. Lebedeva, N.V. Zubovka, M. Pasero, M. Bellezza, S.
472 Merlino and N.V. Chukanov, *Can. Mineral.*, 42 (2004), pp. 723-729
- 473 [16] P.J. Dunn, D.R. Peacor, P.B. Leavens and J.L. Baum, *Am. Mineral.*, 68 (1983),
474 pp. 1033-1037
- 475 [17] C. Gaudfroy and F. Permingeat, *Soc. Franc. Mineral. Crist, Bull.*, 88 (1965), pp.
476 254-262
- 477 [18] S. Merlino and P. Orlandi, *Am. Min.*, 86 (2001), pp. 1293-1301

- 478 [19] S.J. Barnett, C.D. Adams and A.R.W. Jackson, *Cem, Concr. Res.*, 31 (2001), pp.
479 13-17
- 480 [20] R. Buhkert and H.-J. Kuzel, *ZKG Int.*, 24 (1971), pp. 83-85
- 481 [21] H. McMurdie, M. Morris, E. Evans, B. Paretzkin, W. Wong-Ng and Y. Zhang,
482 *Powder Diffraction*, 2 (1987), p. 44
- 483 [22] H. Poellmann, H.J. Kuzel and R.Wenda, *N. Jb. Miner. Abh.*, 160 (1989), pp.
484 133-158
- 485 [23] S.P. Thompson, J.E. Parker, J. Potter, T.P. Hill, A. Birt, T.M. Cobb, F. Yuan, C.C.
486 Tang, *Rev. Sci. Instrum.*, 80 (2009), pp. 075107–075109
- 487 [24] Topas Academic reference
- 488 [25] H.F.W. Taylor, *Cement Chemistry*, Second Edition, Thomas Telford Publishing,
489 London, 1997
- 490 [26] J. Coates, *Interpretation of IR spectra, a practice approach*, *Encyclopedia of*
491 *Chemistry*, J. Wiley and Sons Ltd, Chichester, 2000, pp 10815-10837
- 492 [27] H. Kollmann and G. Strübl, *Chem. Erde.*, 40 (1981), pp. 110-120
- 493
- 494 [28] D. Altermatt and I.D. Brown, *Acta Cryst. B*41 (1985), pp240-244
- 495 [29] J. Aguilera, M.T. Blanco-Valera and T. Vazquez, *Cem. Concr. Res.*, 31 (2001),
496 pp. 1163-1168

1 Table Captions

2

3

4 Table 1 Refined unit cell parameters.

5

6 Table 2 Identification of phases present from analysis of synchrotron powder XRD
7 data and weighted R value from Rietveld refinement of data.

8

9 Table 3 Calculated Bond Lengths from Rietveld refinement of data collected on
10 ettringite-type phases; $\text{Ca}_6[\text{M}(\text{OH})_6 \cdot 12\text{H}_2\text{O}]_2(\text{SO}_4)_3 \cdot 2\text{H}_2\text{O}$, M = Al, Fe, Ga.

11

12 Table 4 Calculated Bond Lengths from Rietveld refinement of data collected on
13 thaumasite-type phases; $\text{Ca}_6[\text{M}(\text{OH})_6 \cdot 12\text{H}_2\text{O}]_2(\text{SO}_4)_2(\text{CO}_3)_2$, M = Mn, Sn.

14

15 Table 5 Cation valences determined using Bond Valence Analysis [28].

16

17 Table 6 Cation-oxygen bond lengths presented as a range of values (top values) and
18 average value (bottom value) for each ettringite and thaumasite type phase.

19

- 20 Table ESI1 Refined atomic positions and thermal parameters of
21 $\text{Ca}_6[\text{Al}(\text{OH})_6 \cdot 12\text{H}_2\text{O}]_2(\text{SO}_4)_3 \cdot 2\text{H}_2\text{O}$, * parameters fixed at values from cif file.
22
- 23 Table ESI2 Refined atomic positions and thermal parameters of
24 $\text{Ca}_6[\text{Fe}(\text{OH})_6 \cdot 12\text{H}_2\text{O}]_2(\text{SO}_4)_3 \cdot 2\text{H}_2\text{O}$, * parameters fixed at values from cif file.
25
- 26 Table ESI3 Refined atomic positions and thermal parameters of
27 $\text{Ca}_6[\text{Ga}(\text{OH})_6 \cdot 12\text{H}_2\text{O}]_2(\text{SO}_4)_3 \cdot 2\text{H}_2\text{O}$, * parameters fixed at values from cif file.
28
- 29 Table ESR4 Refined atomic positions and thermal parameters of
30 $\text{Ca}_6[\text{Mn}(\text{OH})_6 \cdot 12\text{H}_2\text{O}]_2(\text{SO}_4)_2(\text{CO}_3)_2$, * parameters fixed at values from cif file.
31
- 32 Table ESR5 Refined atomic positions and thermal parameters of
33 $\text{Ca}_6[\text{Sn}(\text{OH})_6 \cdot 12\text{H}_2\text{O}]_2(\text{SO}_4)_2(\text{CO}_3)_2$, * parameters fixed at values from cif file.
34
35

36 Figure Captions

37

38

39 Fig.1 (a) ab projection of ettringite: Al(OH)₆ purple, SO₄²⁻ yellow, Ca blue, O pink (b).

40 Projection of ettringite down [11-20].

41

42 Fig.2 Powder XRD patterns of ettringite-type phases.

43

44 Fig.3 IR spectra of ettringite-type phases, red Al, yellow Fe, purple Ga, green Mn,

45 blue Sn and grey CaCO₃.

46

47 Fig. 4 Comparison of ettringite PXRD data with PXRD data collected on thaumasite-

48 type phases.

49

50 Fig. 5 Refined lattice parameters against octahedral cation radii. (a) refined *a*

51 parameter, ■, published ettringite *a* parameter, ◆, [5] published thaumasite *a*

52 parameter, ◆, [7] (b) refined *c* parameter, ▲, published ettringite *c* parameter, , [5],

53 published thaumasite *c* parameter, ●, [7].

54

55 Fig. 6 Average Cation – Oxygen Bond Lengths as a function of cation radius of

56 octahedral site ion. ◆ Ca-O, ▲ M-O, ● S-O, X C-O.

57

58

59

60 Fig. ESI 1 Final observed (blue), calculated (red) and difference (green) profiles from
61 multiphase Rietveld refinement of $\text{Ca}_6[\text{Al}(\text{OH})_6 \cdot 12\text{H}_2\text{O}]_2(\text{SO}_4)_3 \cdot 2\text{H}_2\text{O}$.

62

63 Fig. ESI 2 Final observed (blue), calculated (red) and difference (green) profiles from
64 multiphase Rietveld refinement of $\text{Ca}_6[\text{Fe}(\text{OH})_6 \cdot 12\text{H}_2\text{O}]_2(\text{SO}_4)_3 \cdot 2\text{H}_2\text{O}$.

65

66 Fig. ESI 3 Final observed (blue), calculated (red) and difference (green) profiles from
67 multiphase Rietveld refinement of $\text{Ca}_6[\text{Ga}(\text{OH})_6 \cdot 12\text{H}_2\text{O}]_2(\text{SO}_4)_3 \cdot 2\text{H}_2\text{O}$.

68

69 Fig. ESI 4 Final observed (blue), calculated (red) and difference (green) profiles
70 from multiphase Rietveld refinement of $\text{Ca}_6[\text{Mn}(\text{OH})_6 \cdot 12\text{H}_2\text{O}]_2(\text{SO}_4)_2(\text{CO}_3)_2$.

71

72 Fig. ESI 5 Final observed (blue), calculated (red) and difference (green) profiles from
73 multiphase Rietveld refinement of $\text{Ca}_6[\text{Sn}(\text{OH})_6 \cdot 12\text{H}_2\text{O}]_2(\text{SO}_4)_2(\text{CO}_3)_2$.

74

Analogue	Cation radius (Å)	<i>a</i> (Å)	<i>c</i> (Å)
Al	0.535	11.227(3)	21.466(4)
Mn ^a	0.53	11.071(5)	21.156(8)
Ga	0.62	11.202(2)	21.797(3)
Fe	0.645	11.162(3)	22.04(1)
Sn ^a	0.69	11.066(1)	22.420(1)

^a Refined on thaumasite-type cell in space group . *c* parameter doubled for comparison to ettringite cell.

Composition	Phases present	Rwp
$\text{Ca}_6[\text{Al}(\text{OH})_6 \cdot 12\text{H}_2\text{O}]_2(\text{SO}_4)_3 \cdot 2\text{H}_2\text{O}$	$\text{Ca}_6[\text{Al}(\text{OH})_6 \cdot 12\text{H}_2\text{O}]_2(\text{SO}_4)_3 \cdot 2\text{H}_2\text{O} +$ $\text{CaSO}_4 \cdot 2\text{H}_2\text{O} + \text{Al}_2(\text{SO}_4)_3 \cdot 8\text{H}_2\text{O} +$ CaCO_3	8.060
$\text{Ca}_6[\text{Fe}(\text{OH})_6 \cdot 12\text{H}_2\text{O}]_2(\text{SO}_4)_3 \cdot 2\text{H}_2\text{O}$	$\text{Ca}_6[\text{Fe}(\text{OH})_6 \cdot 12\text{H}_2\text{O}]_2(\text{SO}_4)_3 \cdot 2\text{H}_2\text{O} +$ $\text{CaSO}_4 \cdot 2\text{H}_2\text{O} + \text{CaSO}_4 \cdot 0.5\text{H}_2\text{O} +$ CaCO_3	11.724
$\text{Ca}_6[\text{Ga}(\text{OH})_6 \cdot 12\text{H}_2\text{O}]_2(\text{SO}_4)_3 \cdot 2\text{H}_2\text{O}$	$\text{Ca}_6[\text{Ga}(\text{OH})_6 \cdot 12\text{H}_2\text{O}]_2(\text{SO}_4)_3 \cdot 2\text{H}_2\text{O}$	10.197
$\text{Ca}_6[\text{Mn}(\text{OH})_6 \cdot 12\text{H}_2\text{O}]_2(\text{SO}_4)_2(\text{CO}_3)_2$	$\text{Ca}_6[\text{Mn}(\text{OH})_6 \cdot 12\text{H}_2\text{O}]_2(\text{SO}_4)_2(\text{CO}_3)_2 +$ unknown impurity phase	7.005
$\text{Ca}_6[\text{Sn}(\text{OH})_6 \cdot 12\text{H}_2\text{O}]_2(\text{SO}_4)_2(\text{CO}_3)_2$	$\text{Ca}_6[\text{Sn}(\text{OH})_6 \cdot 12\text{H}_2\text{O}]_2(\text{SO}_4)_2(\text{CO}_3)_2 +$ unknown impurity phase	10.195

<i>Cation</i>	<i>O site</i>	<i>Al</i>	<i>Fe</i>	<i>Ga</i>
M1	O1	1.95(4) x3	2.10(6) x3	1.98(5) x3
	O2	1.85(4) x3	1.67(7) x3	1.95(5) x3
M2	O3	2.02(3) x3	1.90(6) x3	1.97(5) x3
	O4	1.81(4) x3	2.43(6) x3	1.96(5) x3
Ca2	O1	2.40(4)	2.42(6)	2.41(5)
	O1	2.50(4)	2.59(6)	2.50(5)
	O3	2.34(4)	2.49(6)	2.42(5)
	O3	2.54(4)	2.54(6)	2.49(5)
	O6	2.51(5)	2.09(7)	2.43(5)
	O8	2.38(5)	2.6(7)	2.52(5)
	O10	2.58(3)	2.27(4)	2.46(4)
	O12	2.51(3)	2.85(3)	2.69(4)
Ca2	O2	2.46(4)	2.20(6)	2.36(5)
	O2	2.49(5)	2.45(5)	2.47(4)
	O4	2.45(4)	2.42(7)	2.47(6)
	O4	2.46(4)	2.66(6)	2.51(5)
	O5	2.60(5)	2.49(7)	2.28(5)
	O7	2.45(6)	2.67(7)	2.63(5)
	O9	2.71(3)	2.72(3)	2.75(2)
	O11	2.76(3)	2.87(2)	2.71(3)
S1	O13	1.72(7)	1.55(1)	1.49(11)
	O16	1.58(2) x3	1.48(6) x3	1.54(5) x3
S2	O14	1.42(8)	1.18(1)	1.42(7)
	O17	1.86(4) x3	1.51(5) x3	1.67(3) x3

S3	O15	1.59(7)	1.58(1)	1.58(9)
	O18	1.41(2) x3	1.80(6) x3	1.51(3) x3

<i>Cation</i>	<i>O site</i>	<i>Mn</i>	<i>Sn</i>
M1	O7	1.94(3) x3	2.16(2) x3
	O8	1.91(3) x3	1.89(2) x3
Ca1	O1	2.49(3)	2.48(2)
	O2	2.53(3)	2.56(2)
	O3	2.32(3)	2.42(3)
	O4	2.48(3)	2.51(3)
	O7	2.68(4)	2.57(3)
	O7	2.73(4)	2.66(3)
	O8	2.22(4)	2.40(3)
	O8	2.23(4)	2.45(3)
S1	O6	1.70(2) x3	1.72(2) x3
	O9	1.47(3)	1.45(4)
C1	O5	1.29 x3 (fixed)	1.24(2) x3

Octahedral cation	M1	M2	Ca1	Ca2	S1	S2	S3	C1
Al [5]	3.23	3.33	2.34	2.01	5.82	5.92	5.9	
Al	2.69	3.24	1.82	2.13	5.84	5.87	5.84	
Fe	4.15	2.81	2.17	2.07	5.71	5.83	5.67	
Ga	3.18	3.18	1.99	1.94	5.2	4.39	5.2	
Mn	3.77		2.36		3.96			3.93
Sn	4.63		1.91		3.9			4.5

	Al	Fe	Ga	Mn	Sn
Ca1-O	2.38-2.78 2.54	2.31-2.92 2.52	2.41-2.69 2.49	2.22-2.73 2.46	2.40-2.66 2.51
Ca2-O	2.33-2.62 2.47	2.32-2.79 2.51	2.36-2.75 2.52		
M1-O	1.82-2.05 1.94	1.73-2.2 1.97	1.95-1.98 1.97	1.91-1.94 1.93	1.89-2.16 2.03
M2-O	1.74-2.00 1.87	2.01-2.07 2.04	1.96-1.97 1.97		
S1-O	1.44-1.50 1.49	1.47-1.50 1.49	1.49-1.54 1.53	1.47-1.70 1.64	1.45-1.72 1.65
S2-O	1.46-1.49 1.48	1.48-1.50 1.5	1.42-1.67 1.61		
S3-O	1.44-1.50 1.49	1.28-1.50 1.5	1.51-1.58 1.53		
C1-O				1.29 1.29	1.24 1.24

site	x	y	z	occupancy	beq
Al1	0	0	0	1	1.4(4)
Al2	0	0	0.25	1	0.9(4)
Ca1	0.002(1)	0.812(1)	0.8697(8)	1	1.6(2)
Ca2	0.997(1)	0.191(1)	0.1195(8)	1	1.5(2)
O1	1.004(3)	0.153(2)	0.938(1)	1	1.67(8)
O2	0.001(4)	0.862(3)	0.050(1)	1	1.67(8)
O3	1.001(2)	0.133(2)	0.793(1)	1	1.67(8)
O4	-0.001(3)	0.876(2)	0.186(2)	1	1.67(8)
O5	1.008(3)	0.345(3)	0.044(2)	1	1.67(8)
O6	0.006(2)	0.645(2)	0.950(1)	1	1.67(8)
O7	0.012(2)	0.360(2)	0.197(1)	1	1.67(8)
O8	0.988(2)	0.644(2)	0.778(1)	1	1.67(8)
O9	0.236(2)	0.394(2)	0.621(1)	1	1.67(8)
O10	0.726(2)	0.620(2)	0.369(1)	1	1.67(8)
O11	0.248(2)	0.400(2)	0.134(1)	1	1.67(8)
O12	0.751(2)	0.589(2)	0.852(1)	1	1.67(8)
O13	0.33333	0.66667	0.425*	1	8.5(2)
O14	0.33333	0.66667	0.819*	1	8.5(2)
O15	0.33333	0.66667	0.076	1	8.5(2)
O16	0.195	0.628	0.519	1	8.5(2)
O17	0.195*	0.620*	0.724*	1	8.5(2)
O18	0.192*	0.585*	0.982*	1	8.5(2)
O19	0.227*	0.685*	0.243*	0.667	1.6(1)
S1	0.33333	0.66667	0.492*	1	2.5(1)
S2	0.33333	0.66667	0.751*	1	2.5(1)
S3	0.33333	0.66667	0.009*	1	2.5(1)

site	x	y	z	occupancy	beq
Fe1	0	0	0.007(2)	1	1.7(4)
Fe2	0	0	0.249(1)	1	1.0(4)
Ca1	0.017(1)	0.818(1)	0.877(1)	1	1.1(4)
Ca2	0.990(2)	0.190(2)	0.122(1)	1	1.2(4)
O1	0.999(4)	0.156(3)	0.946(2)	1	1.1(2)
O2	0.012(5)	0.888(4)	0.057(2)	1	1.1(2)
O3	0.983(4)	0.132(4)	0.805(2)	1	1.1(2)
O4	0.001(4)	0.854(4)	0.191(2)	1	1.1(2)
O5	0.994(5)	0.335(5)	0.038(3)	1	2.5(2)
O6	0.004(4)	0.666(4)	0.953(2)	1	2.5(2)
O7	-0.004(5)	0.353(4)	0.197(2)	1	2.5(2)
O8	0.995(4)	0.650(4)	0.789(2)	1	2.5(2)
O9	0.284(3)	0.414(3)	0.620(2)	1	2.5(2)
O10	0.767(3)	0.605(3)	0.370(2)	1	2.5(2)
O11	0.239(3)	0.411(5)	0.135(2)	1	2.5(2)
O12	0.739(4)	0.583(5)	0.860(2)	1	2.5(2)
O13	0.33333	0.66667	0.425*	1	7.9(5)
O14	0.33333	0.66667	0.819*	1	7.9(5)
O15	0.33333	0.66667	0.076	1	7.9(5)
O16	0.195	0.628	0.519	1	7.9(5)
O17	0.195*	0.620*	0.724*	1	7.9(5)
O18	0.192*	0.585*	0.982*	1	7.9(5)
O19	0.209(3)	0.661(4)	0.240(2)	0.667	1.0*
S1	0.33333	0.66667	0.492*	1	2.0(2)
S2	0.33333	0.66667	0.751*	1	2.0(2)
S3	0.33333	0.66667	0.009*	1	2.0(2)

site	x	y	z	occupancy	beq
Ga1	0	0	0	1	1.4(2)
Ga2	0	0	0.25	1	1.0(2)
Ca1	0.006(2)	0.811(2)	0.876(1)	1	2.6(3)
Ca2	0.989(1)	0.189(1)	0.1228(8)	1	1.0(2)
O1	1.001(4)	0.142(5)	0.946(2)	1	1.9(9)
O2	0.000(5)	0.864(4)	0.056(2)	1	0.9(9)
O3	0.999(4)	0.138(5)	0.806(2)	1	1.4(9)
O4	0.004(5)	0.864(4)	0.195(2)	1	1.9(9)
O5	0.992(5)	0.332(5)	0.048(2)	1	2.6(9)
O6	0.003(5)	0.670(3)	0.961(2)	1	2.0(8)
O7	0.013(4)	0.353(4)	0.214(2)	1	3.3(9)
O8	0.991(4)	0.634(3)	0.801(2)	1	2.4(7)
O9	0.279(2)	0.412(2)	0.628(2)	1	3.0(7)
O10	0.763(3)	0.599(3)	0.376(2)	1	1.6(8)
O11	0.253(3)	0.397(3)	0.135(2)	1	3.6(1.0)
O12	0.756(4)	0.585(3)	0.861(2)	1	2.3(1.0)
O13	0.33333	0.66667	0.423(5)	1	6.5(3.2)
O14	0.33333	0.66667	0.814(2)	1	5.2(1.8)
O15	0.33333	0.66667	0.077(4)	1	4.6(2.4)
O16	0.195(4)	0.637(5)	0.520(2)	1	5.1(1.2)
O17	0.177(2)	0.634(4)	0.725(2)	1	6.9(1.2)
O18	0.185(3)	0.588(4)	0.983(2)	1	4.8(1.0)
O19	0.230(3)	0.647(5)	0.247(3)	0.667	5.7(1.2)
S1	0.33333	0.66667	0.491(1)	1	1.8(1.0)
S2	0.33333	0.66667	0.749(2)	1	1.5(5)
S3	0.33333	0.66667	0.005(2)	1	2.4(9)

site	x	y	z	occupancy	beq
Ca1	0.197(1)	0.996(2)	0.267(2)	1	3.2(2)
Mn1	0	0	0.004(2)	1	4.6(3)
C1	0.33333	0.66667	0.4623*	1	1*
S1	0.33333	0.66667	0.98382*	1	0.2(4)
O1	0.398(3)	0.234(4)	0.227(3)	1	1.4(2)
O2	0.248(3)	0.406(3)	0.252(4)	1	1.4(2)
O3	-0.014(3)	0.299(2)	0.079(2)	1	1.4(2)
O4	0.022(3)	0.361(2)	0.439(3)	1	1.4(2)
O5	0.20088	0.623	0.45809	1	1.4(2)
O6	0.174(2)	0.624(2)	0.041(2)	1	1.4(2)
O7	0.152(3)	0.152(3)	0.096(3)	1	1.4(2)
O8	0.120(3)	0.118(3)	0.374(2)	1	1.4(2)
O9	0.33333	0.66667	0.845(3)	1	1.4(2)

site	x	y	z	occupancy	beq
Ca1	0.2104(7)	1.006(1)	0.209(2)	1	1.83(9)
Sn1	0	0	-0.044(2)	1	1.61(5)
C1	0.33333	0.66667	0.485(2)	1	1*
S1	0.33333	0.66667	0.945(2)	1	1*
O1	0.420(2)	0.240(2)	0.184(2)	1	1.4(2)
O2	0.246(2)	0.407(2)	0.208(3)	1	1.4(2)
O3	-0.024(2)	0.336(2)	0.044(2)	1	1.4(2)
O4	0.009(2)	0.345(2)	0.389(2)	1	1.4(2)
O5	0.2394(8)	0.641(2)	0.413(1)	1	1*
O6	0.172(1)	0.625(2)	0.0003(8)	1	5.6(5)
O7	0.159(2)	0.158(2)	0.068(2)	1	0.7(2)
O8	0.113(2)	0.120(2)	0.333(2)	1	0.7(2)
O9	0.33333	0.66667	0.816(3)	1	5.6(5)

Figure
[Click here to download high resolution image](#)

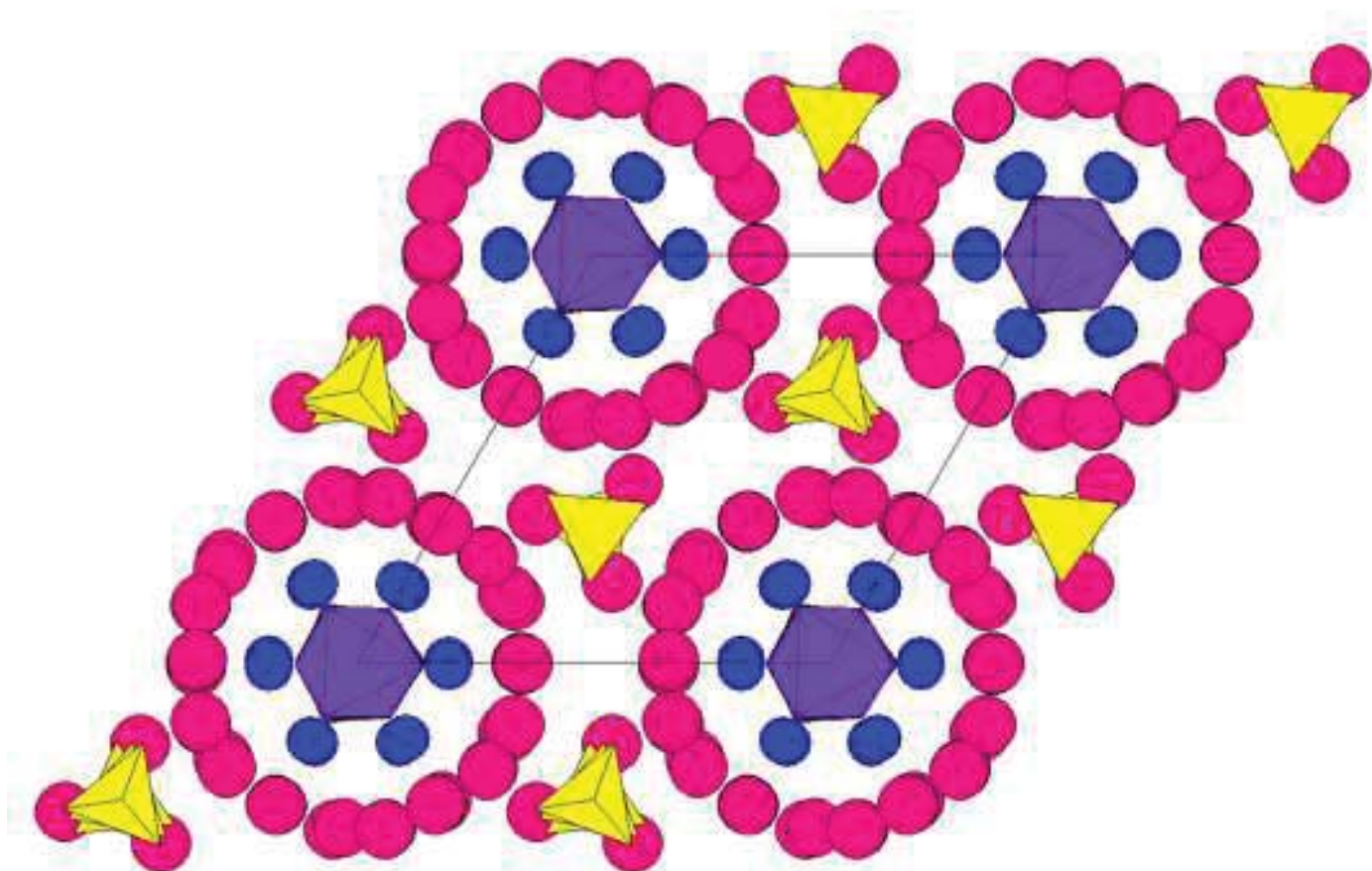


Figure
[Click here to download high resolution image](#)

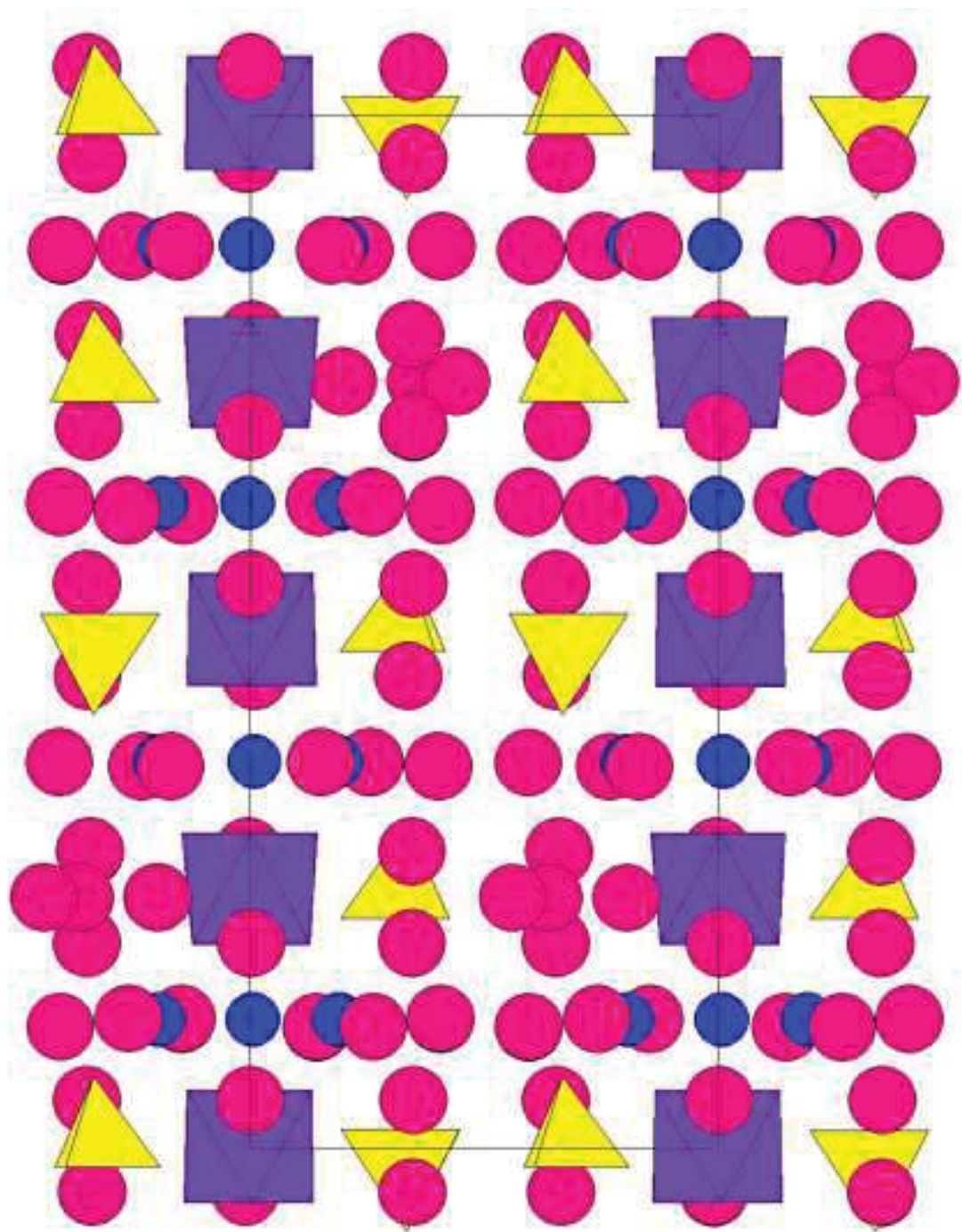


Figure
[Click here to download high resolution image](#)

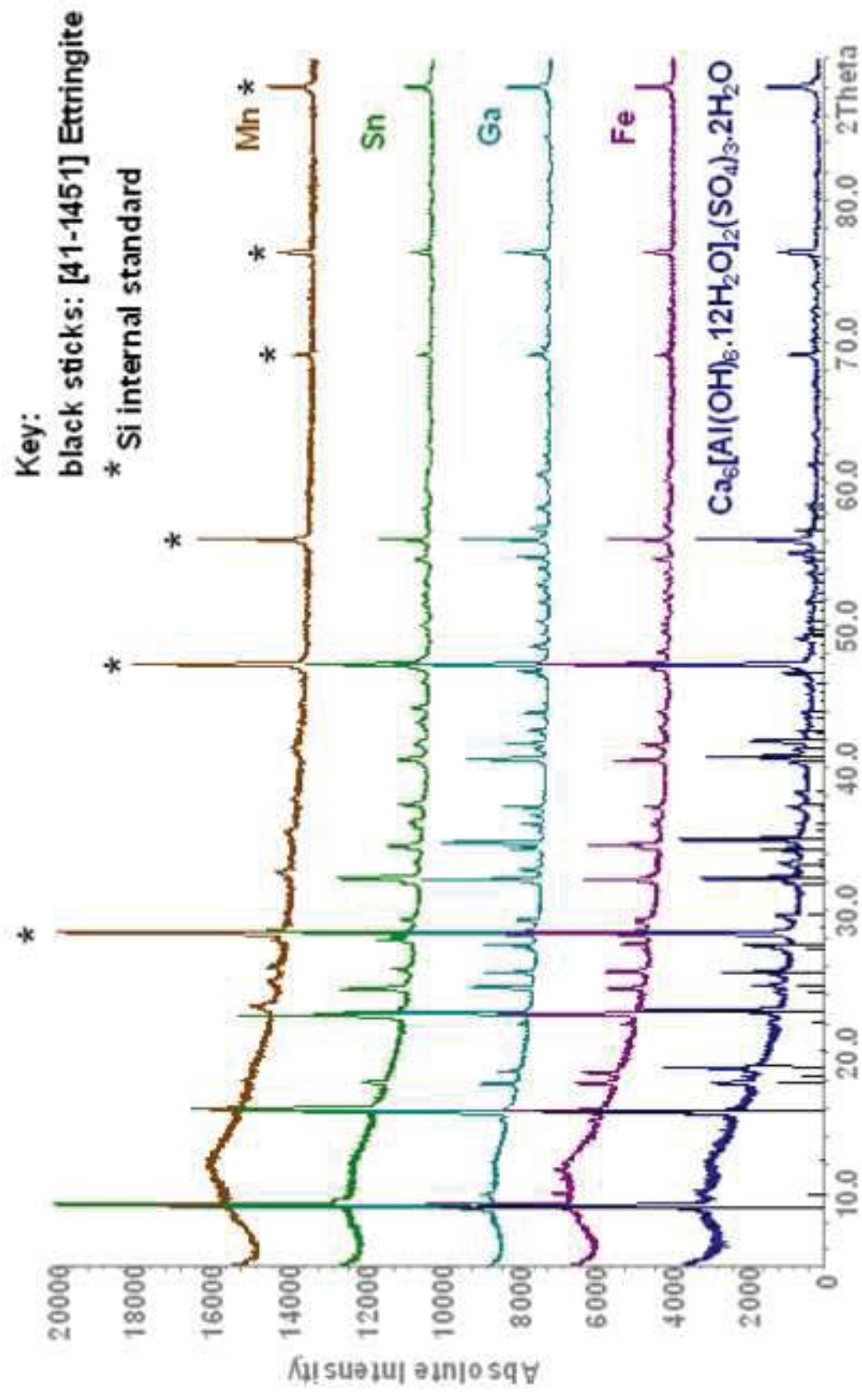


Figure
[Click here to download high resolution image](#)

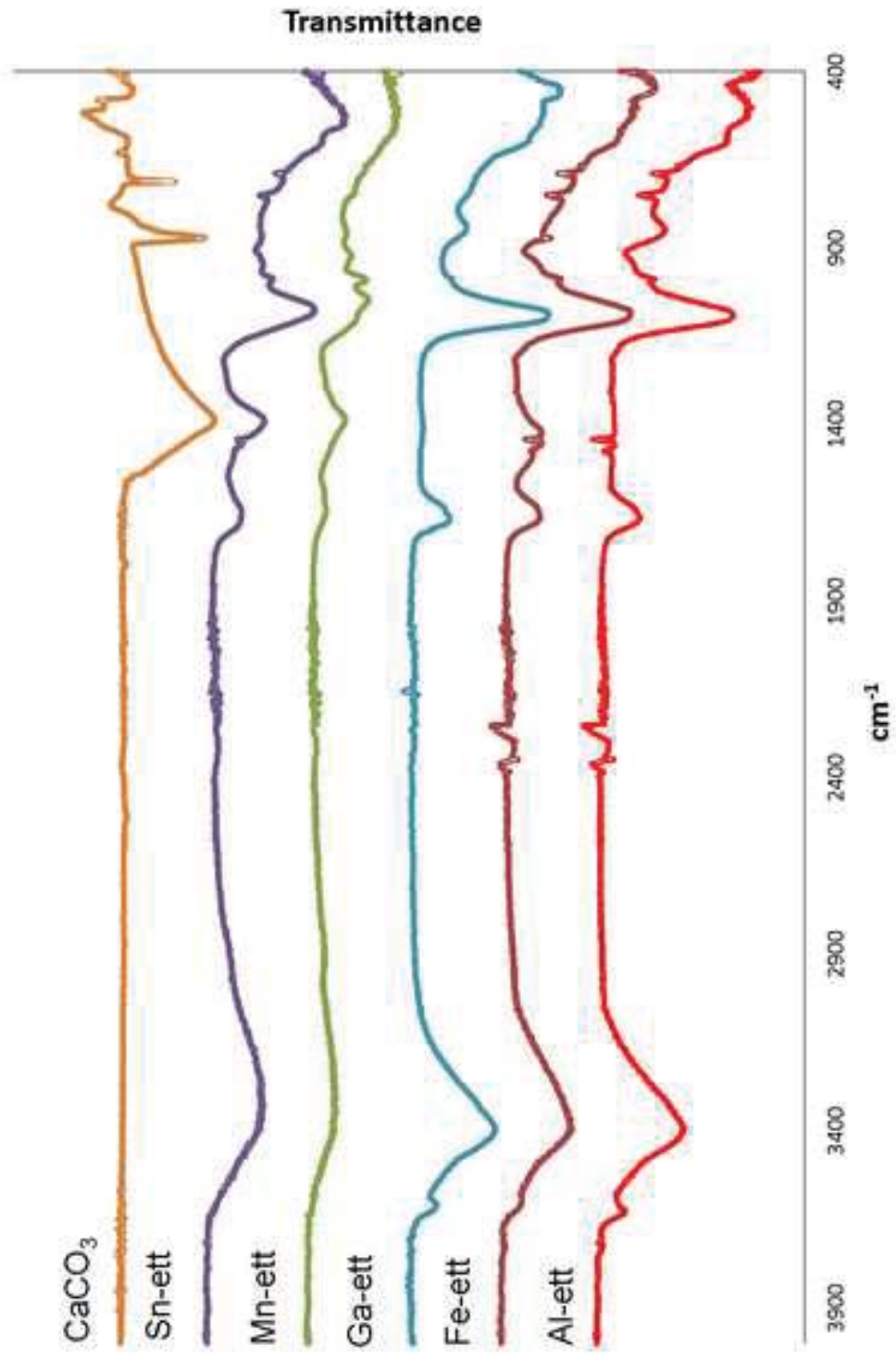


Figure
Click here to download high resolution image

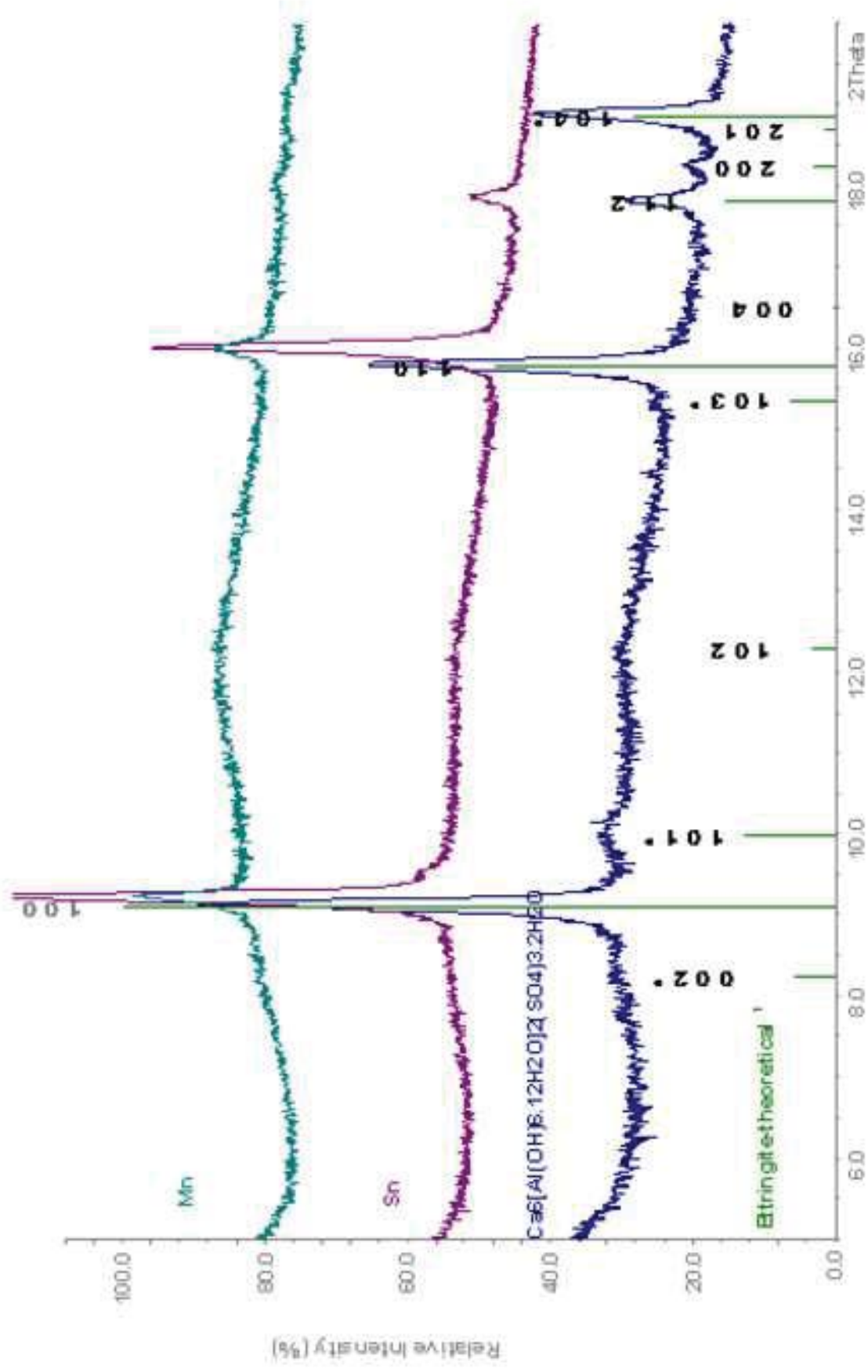


Figure
[Click here to download high resolution image](#)

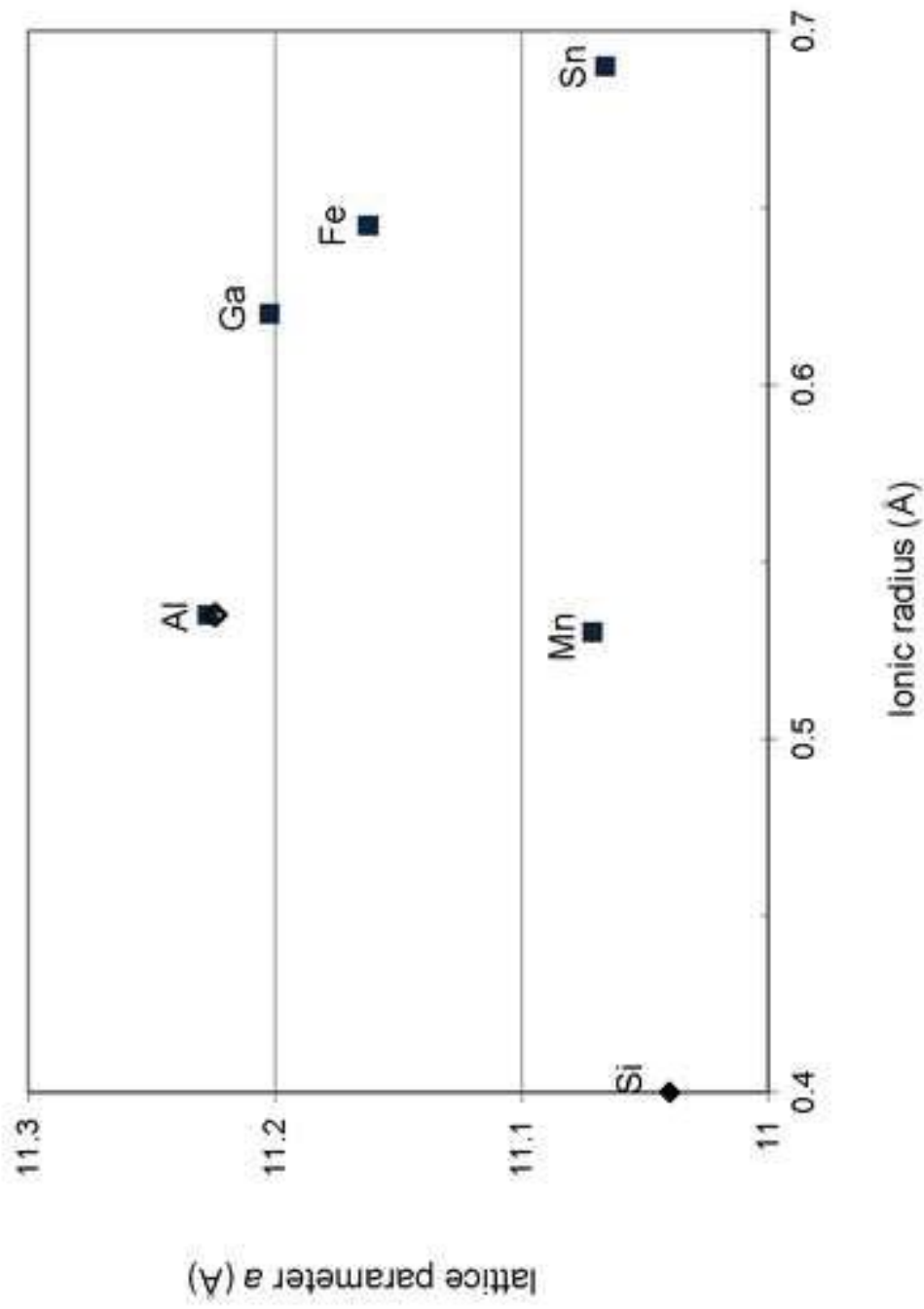


Figure
[Click here to download high resolution image](#)

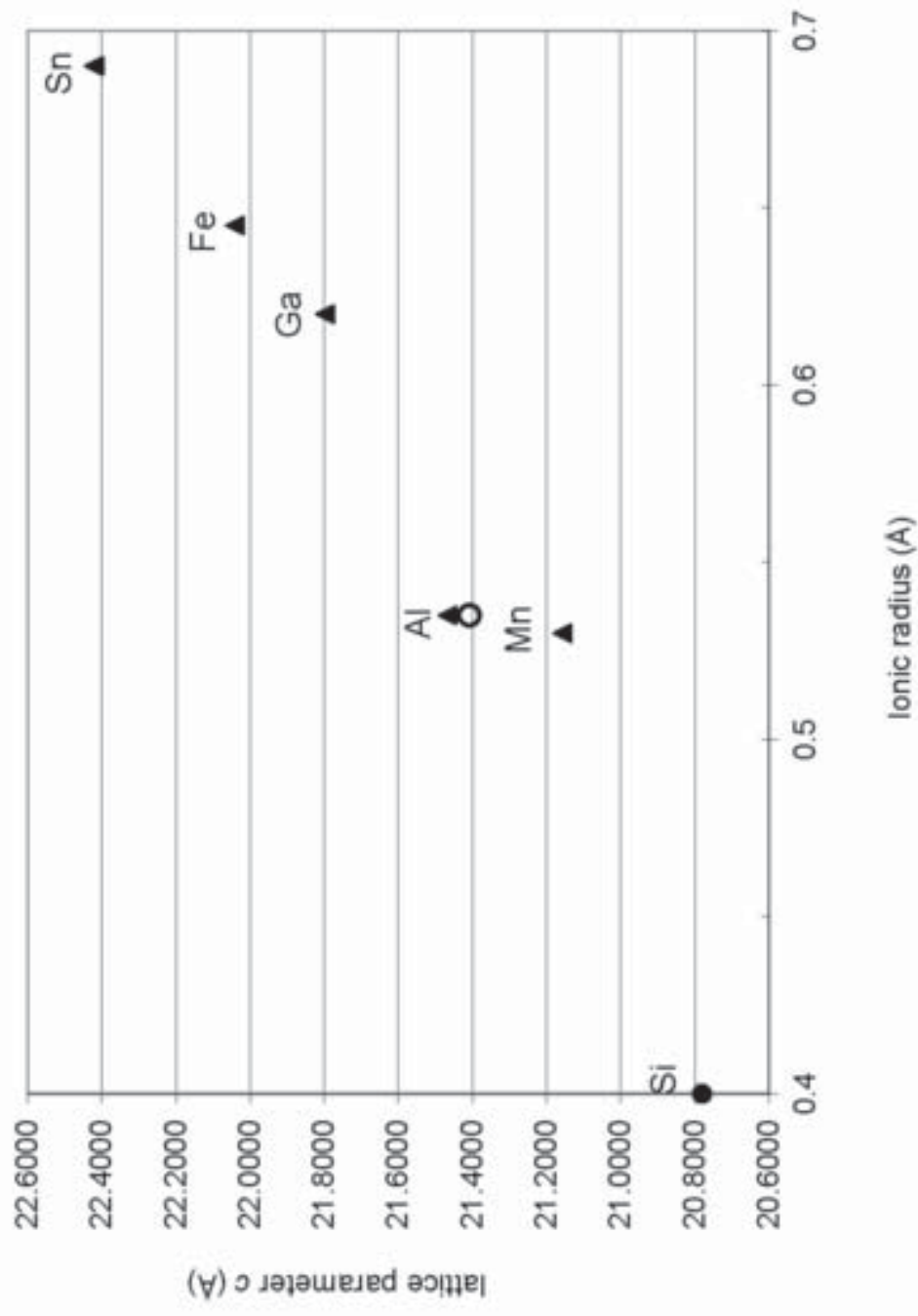


Fig 6.tif
[Click here to download high resolution image](#)

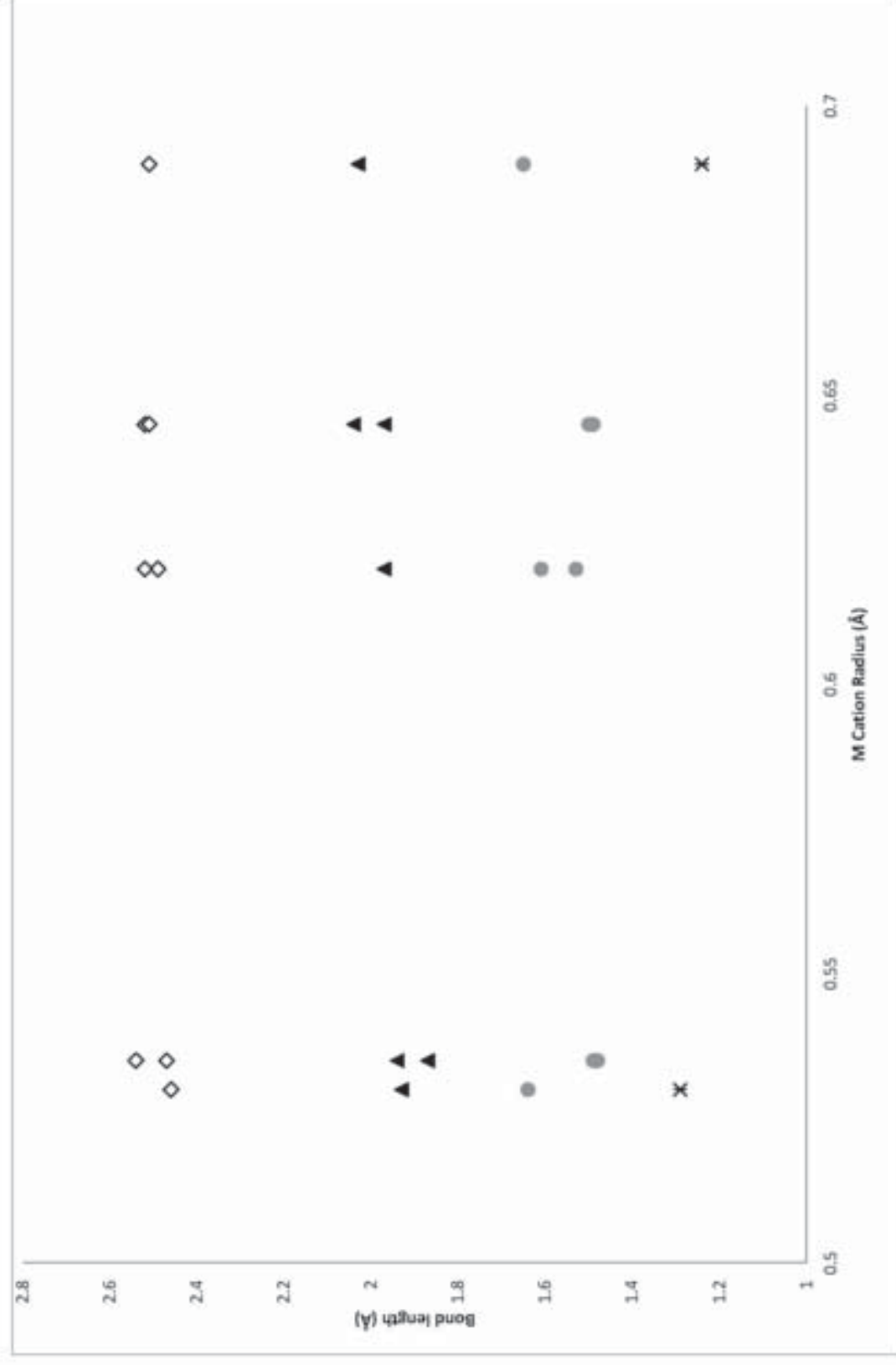


Figure
[Click here to download high resolution image](#)

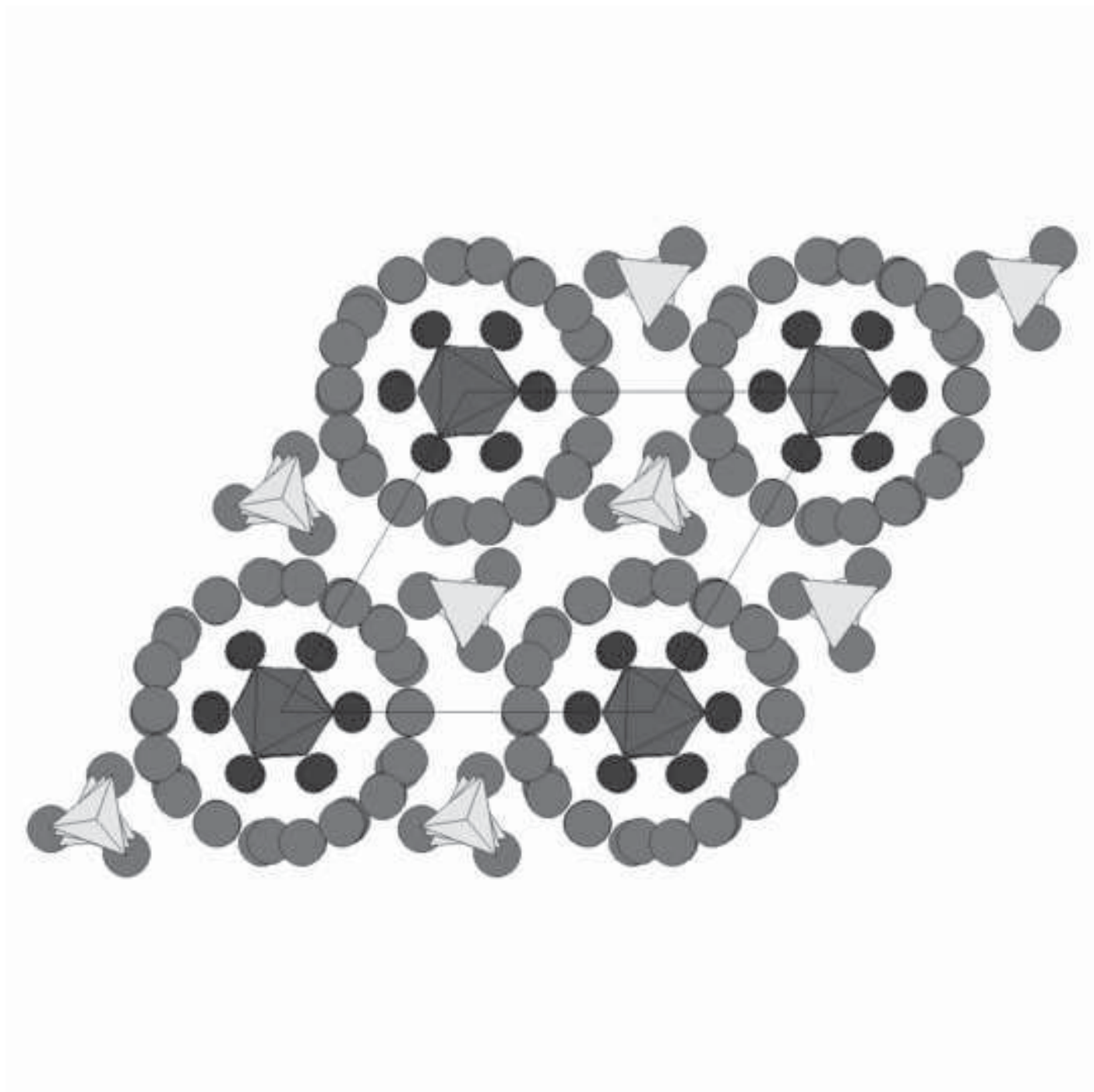


Figure
[Click here to download high resolution image](#)

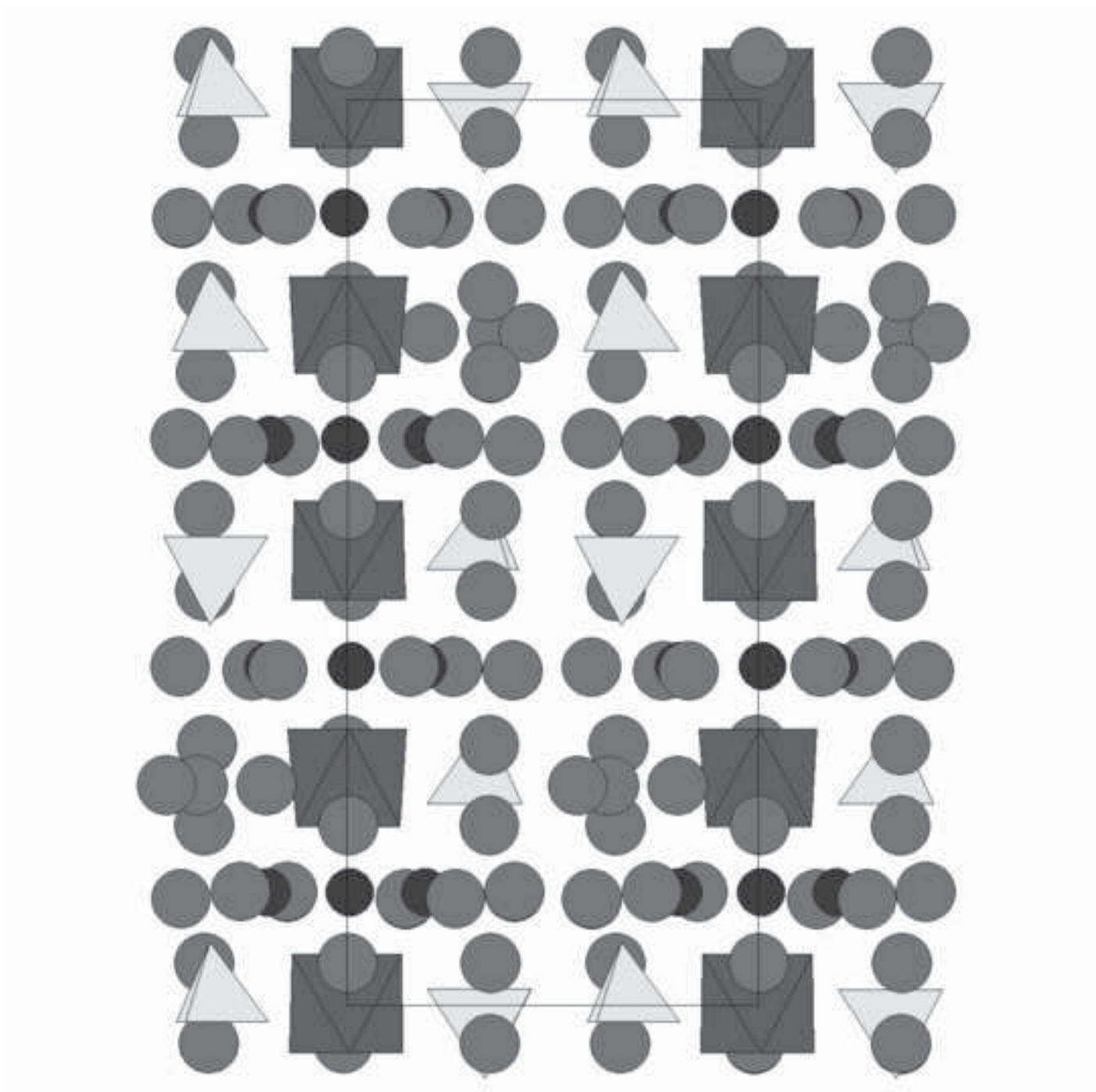


Figure
[Click here to download high resolution image](#)

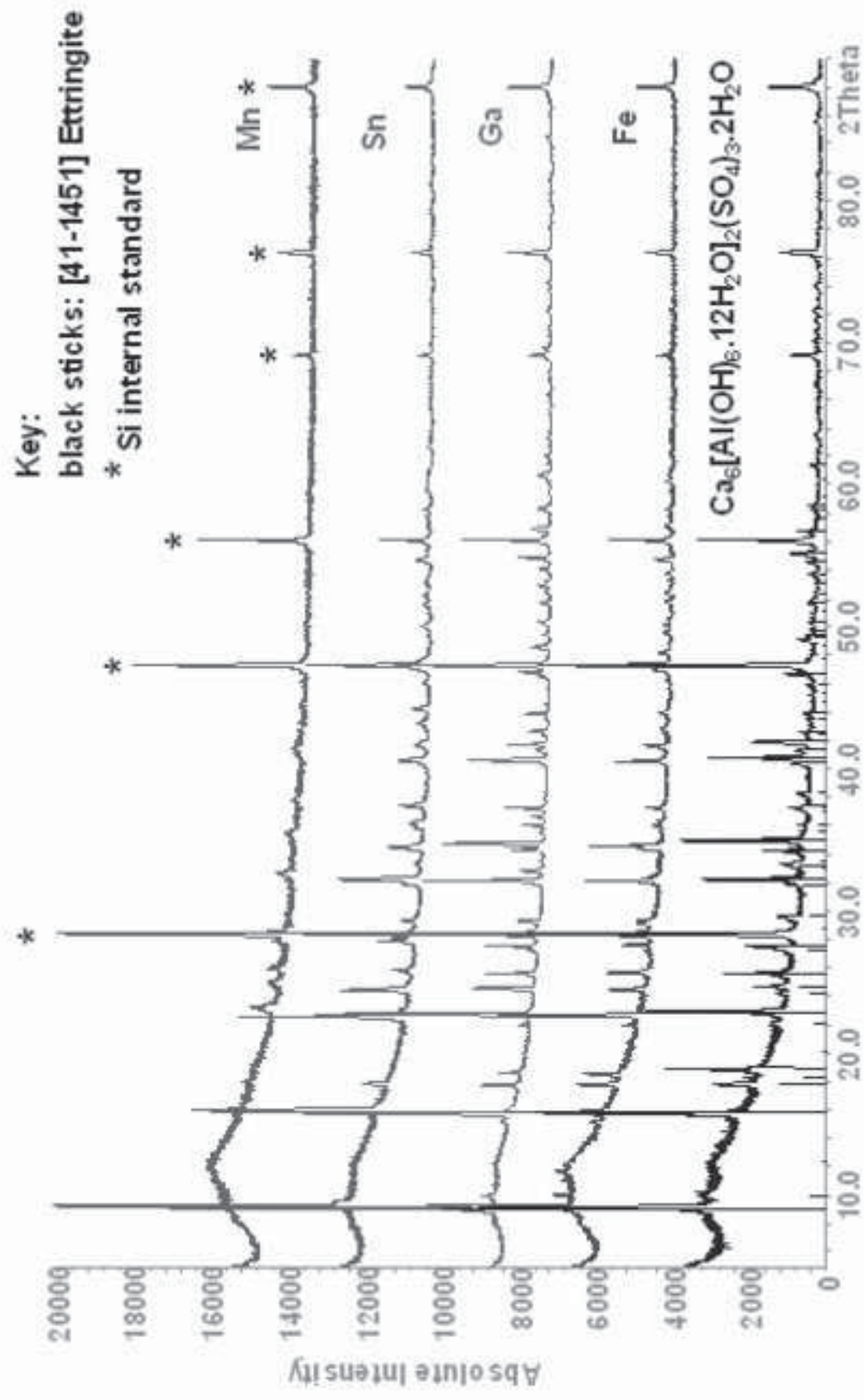


Figure
[Click here to download high resolution image](#)

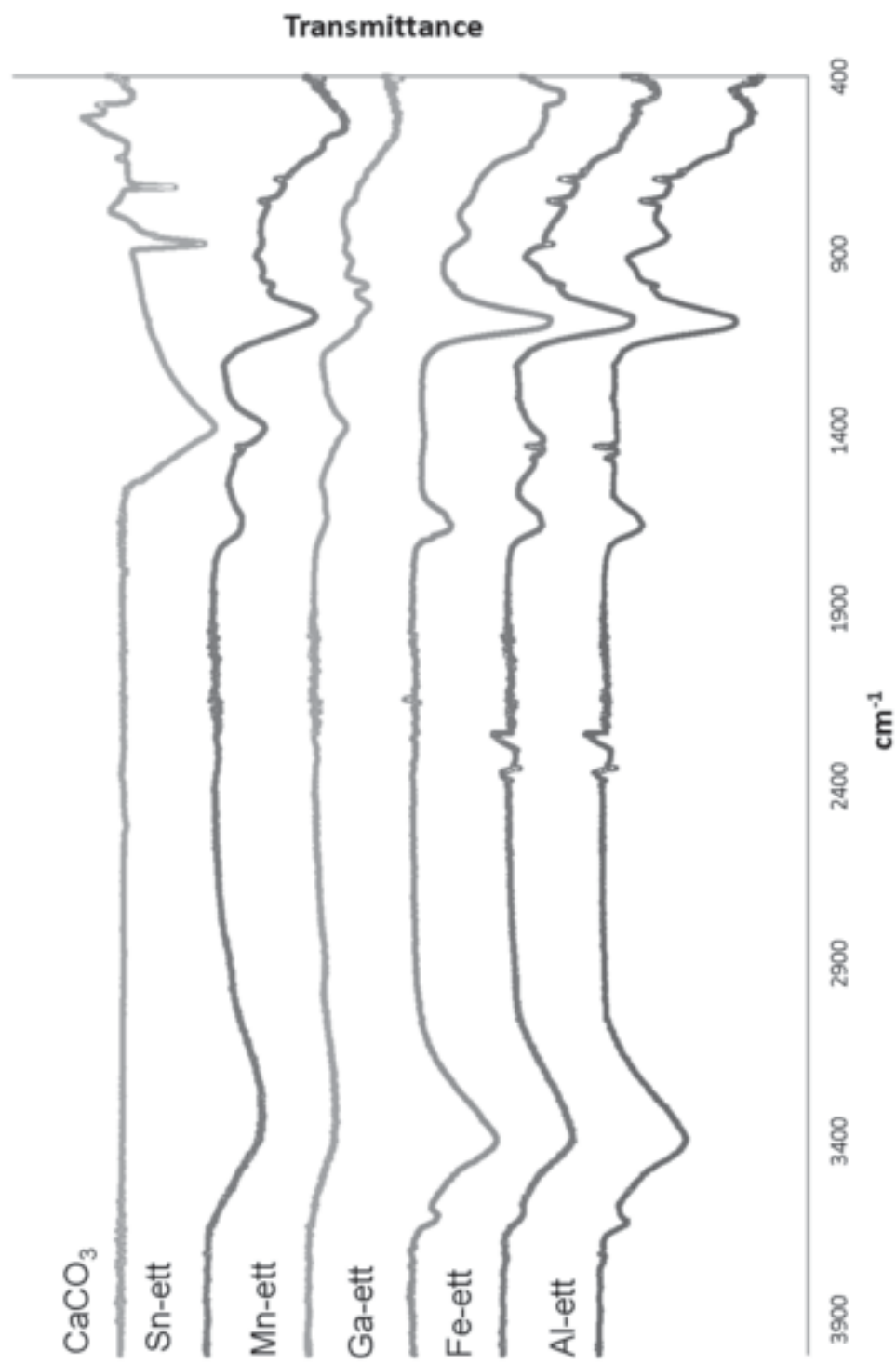


Figure
[Click here to download high resolution image](#)

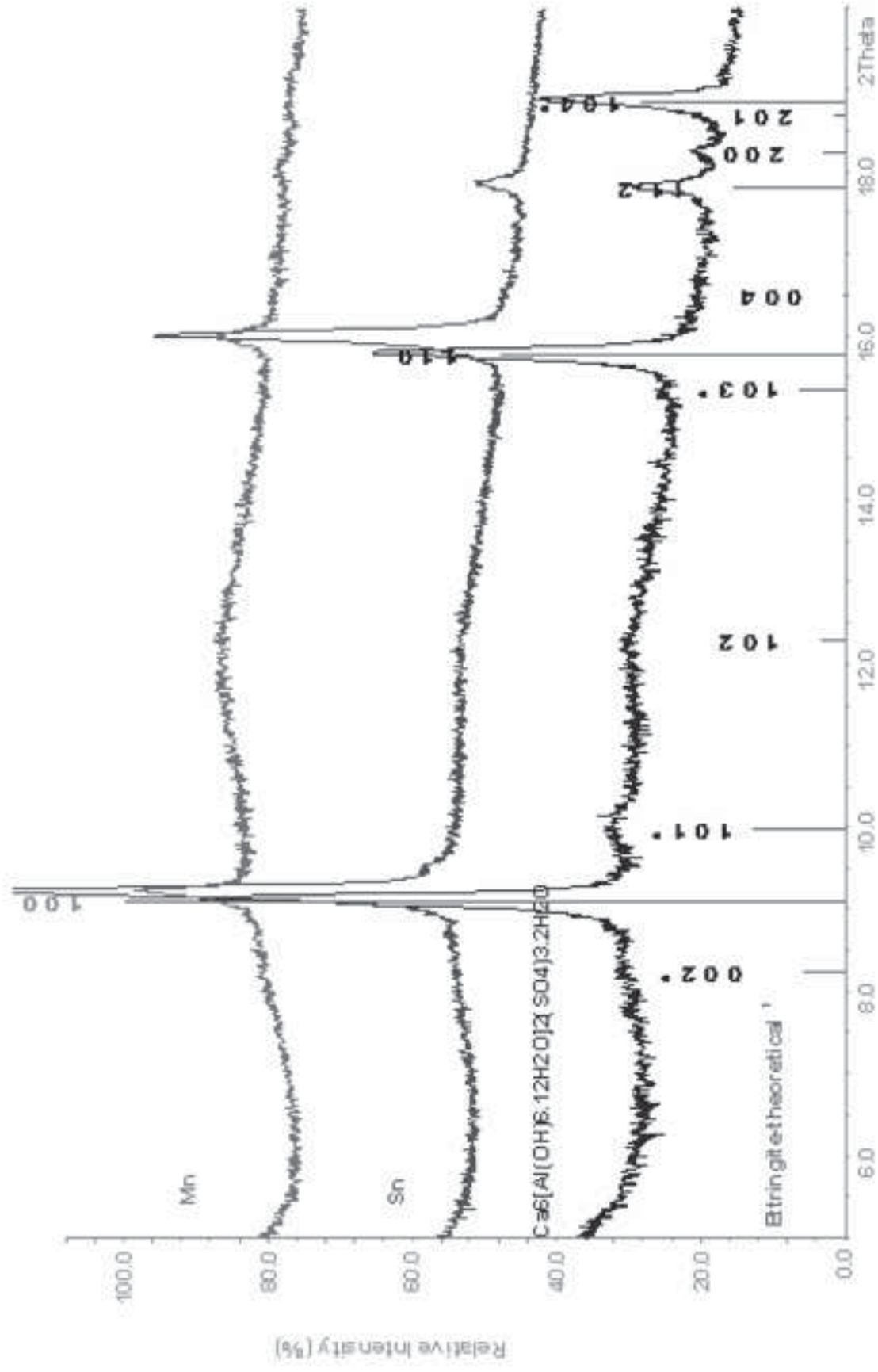


Fig ES11 - .jpg
[Click here to download high resolution image](#)

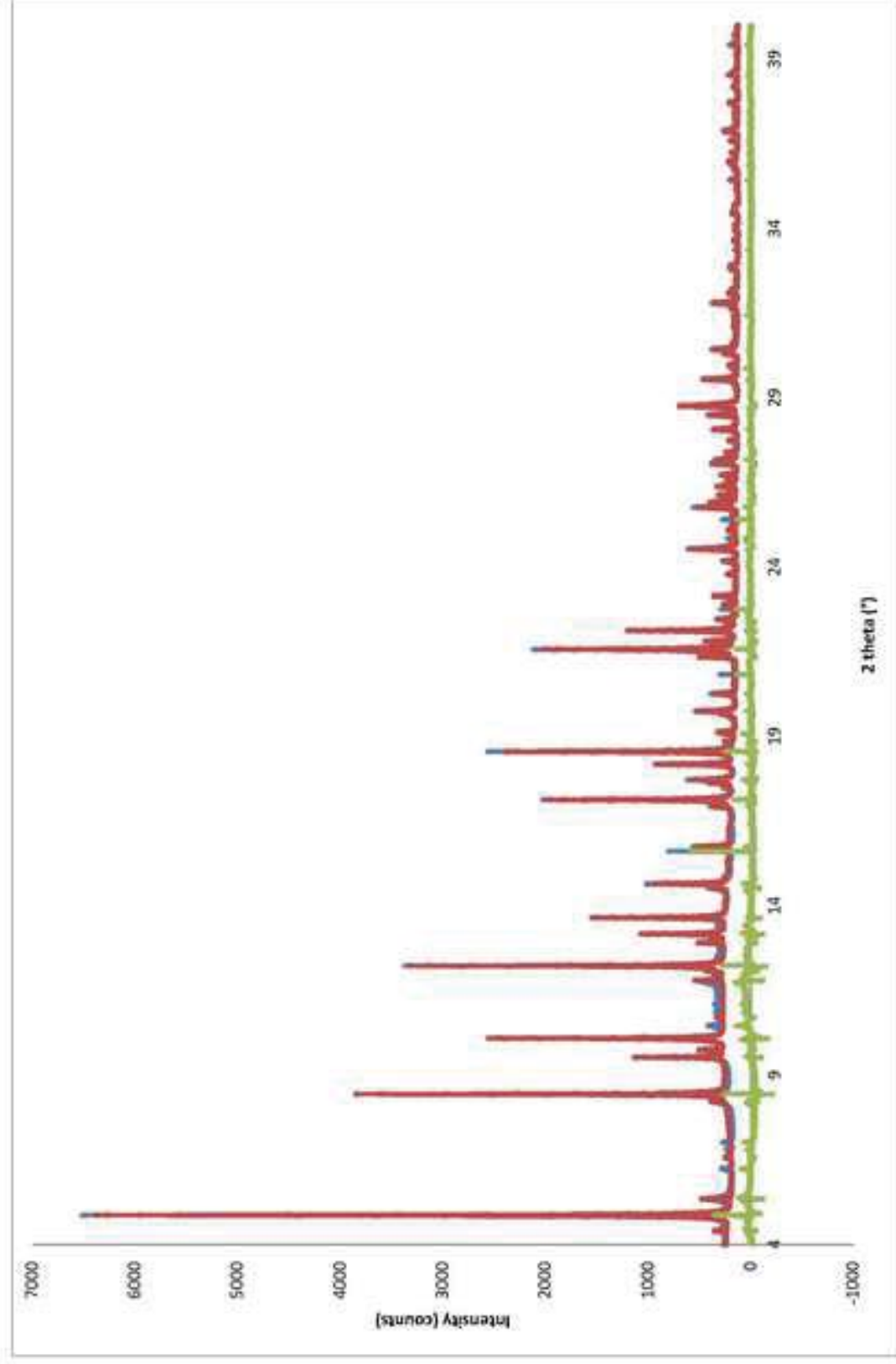


Fig ES12.jpg
[Click here to download high resolution image](#)

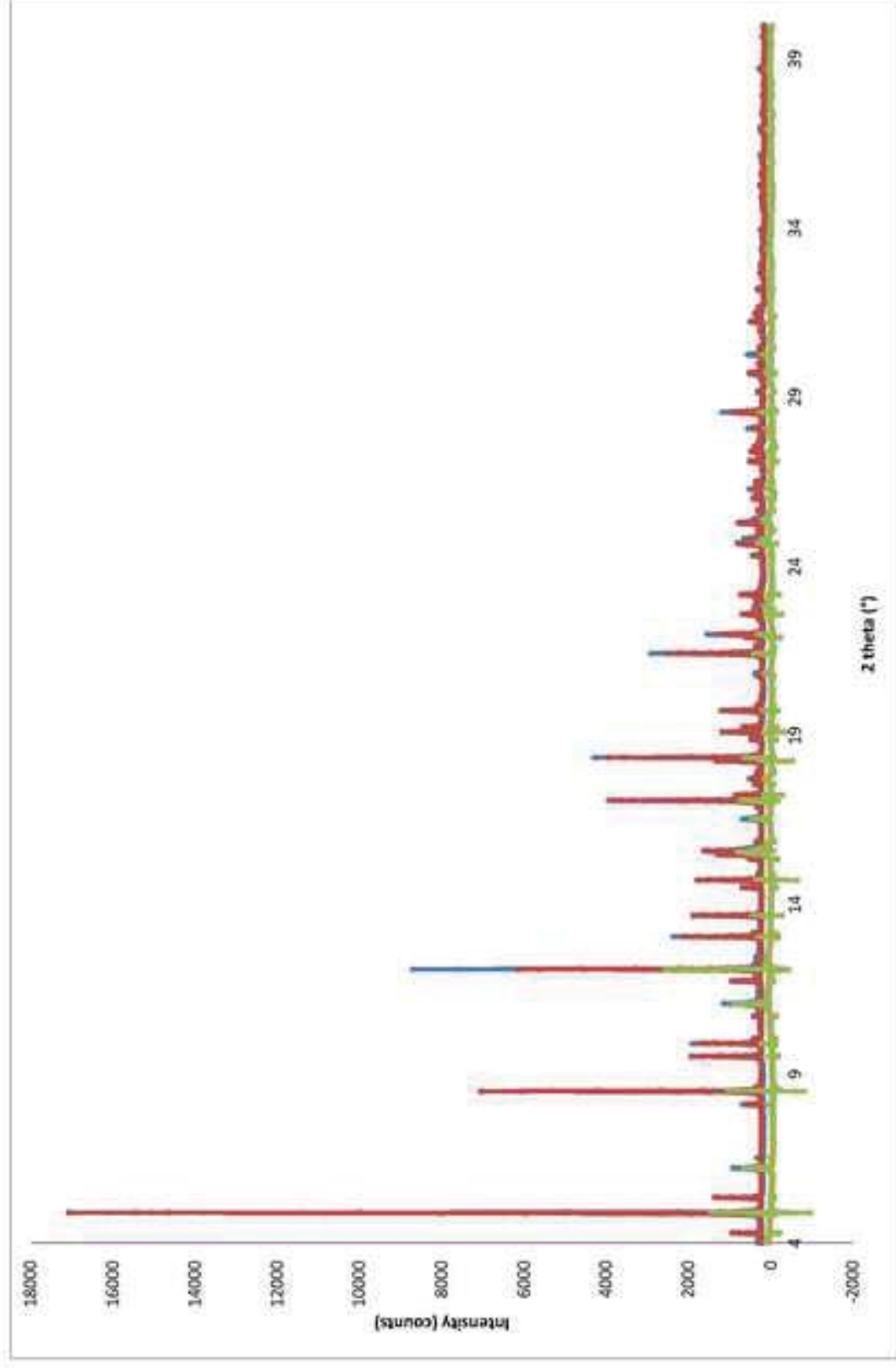


Fig ES13.jpg
[Click here to download high resolution image](#)

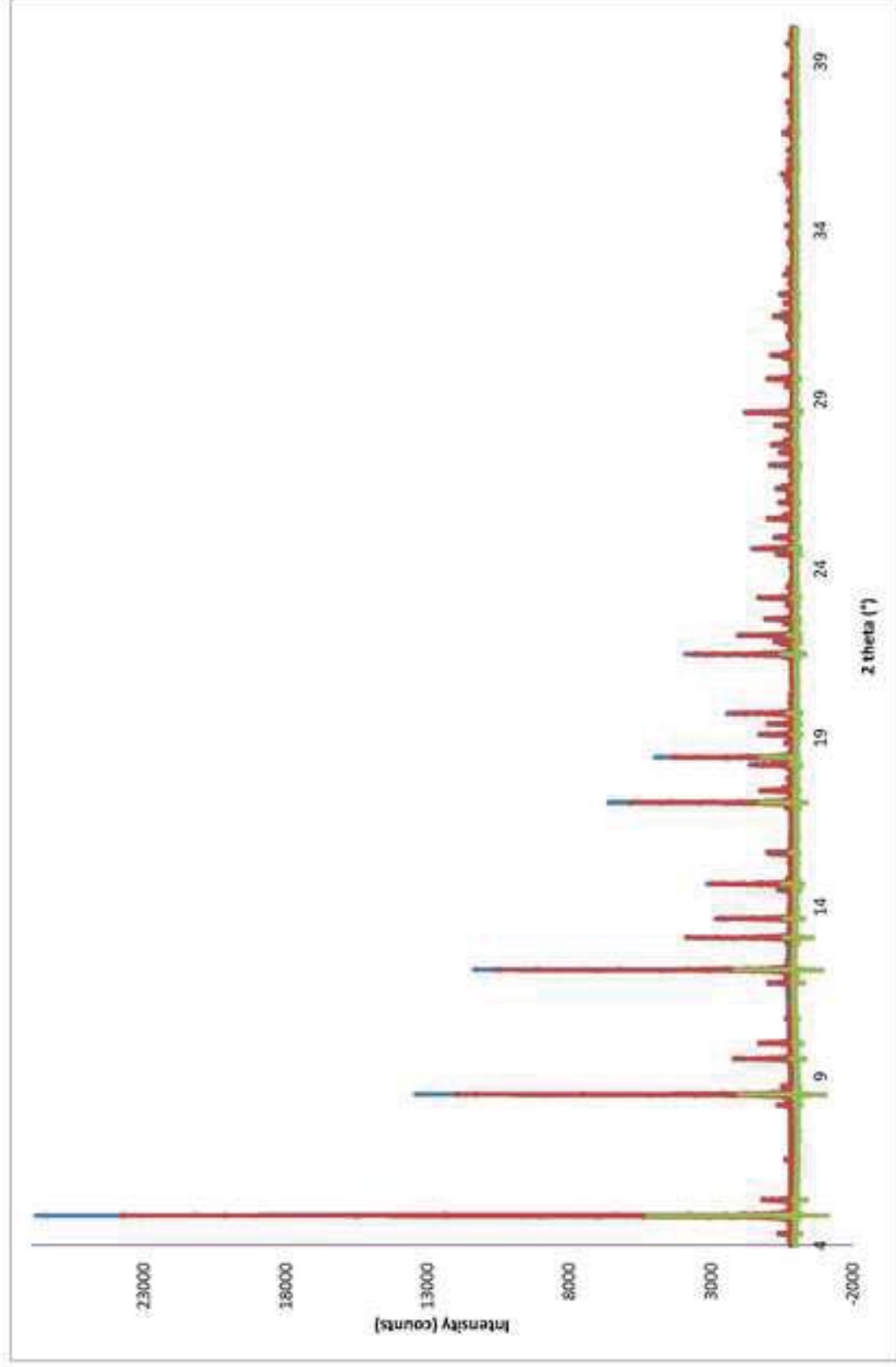


Fig ES14.jpg
[Click here to download high resolution image](#)

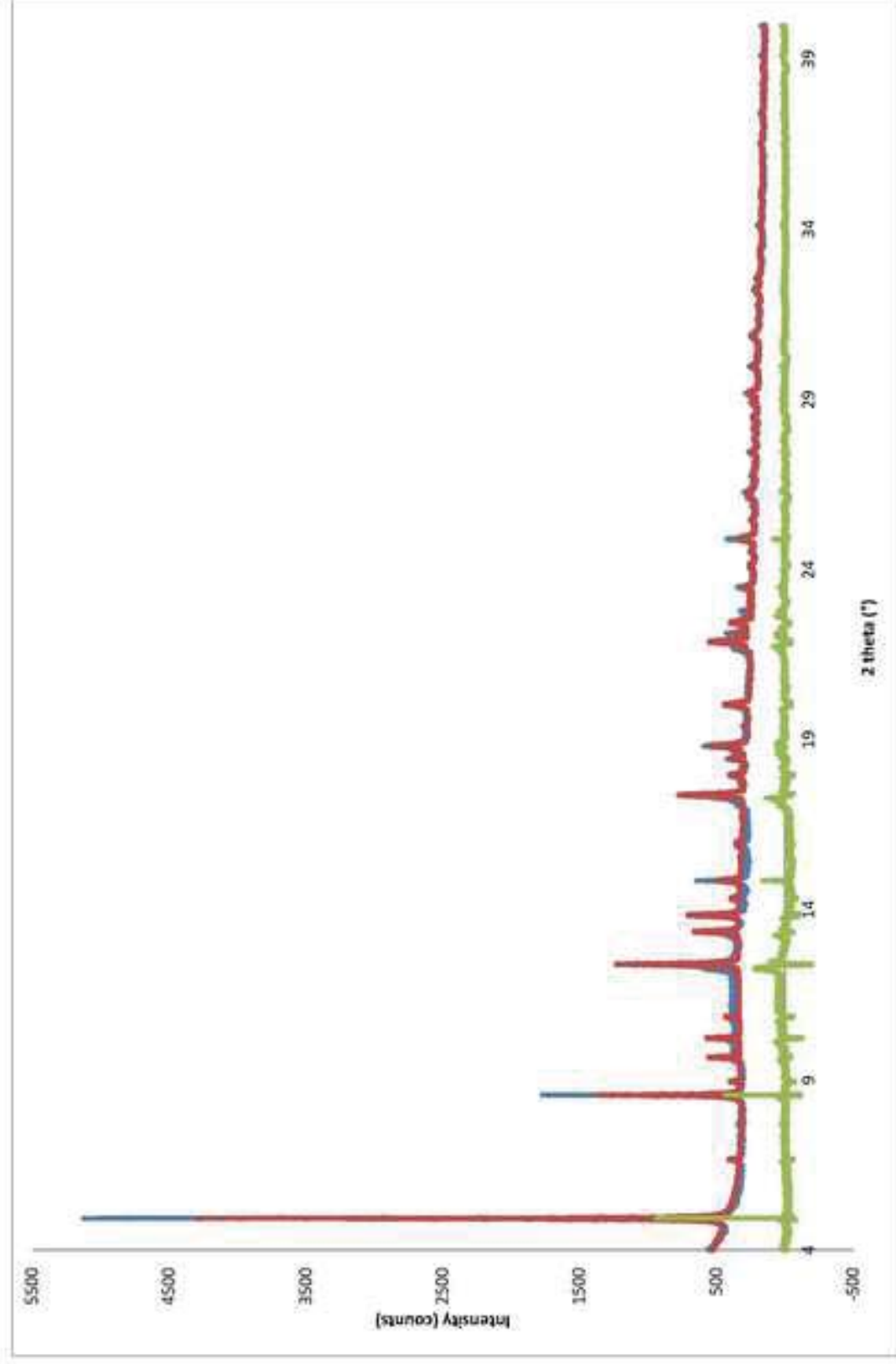
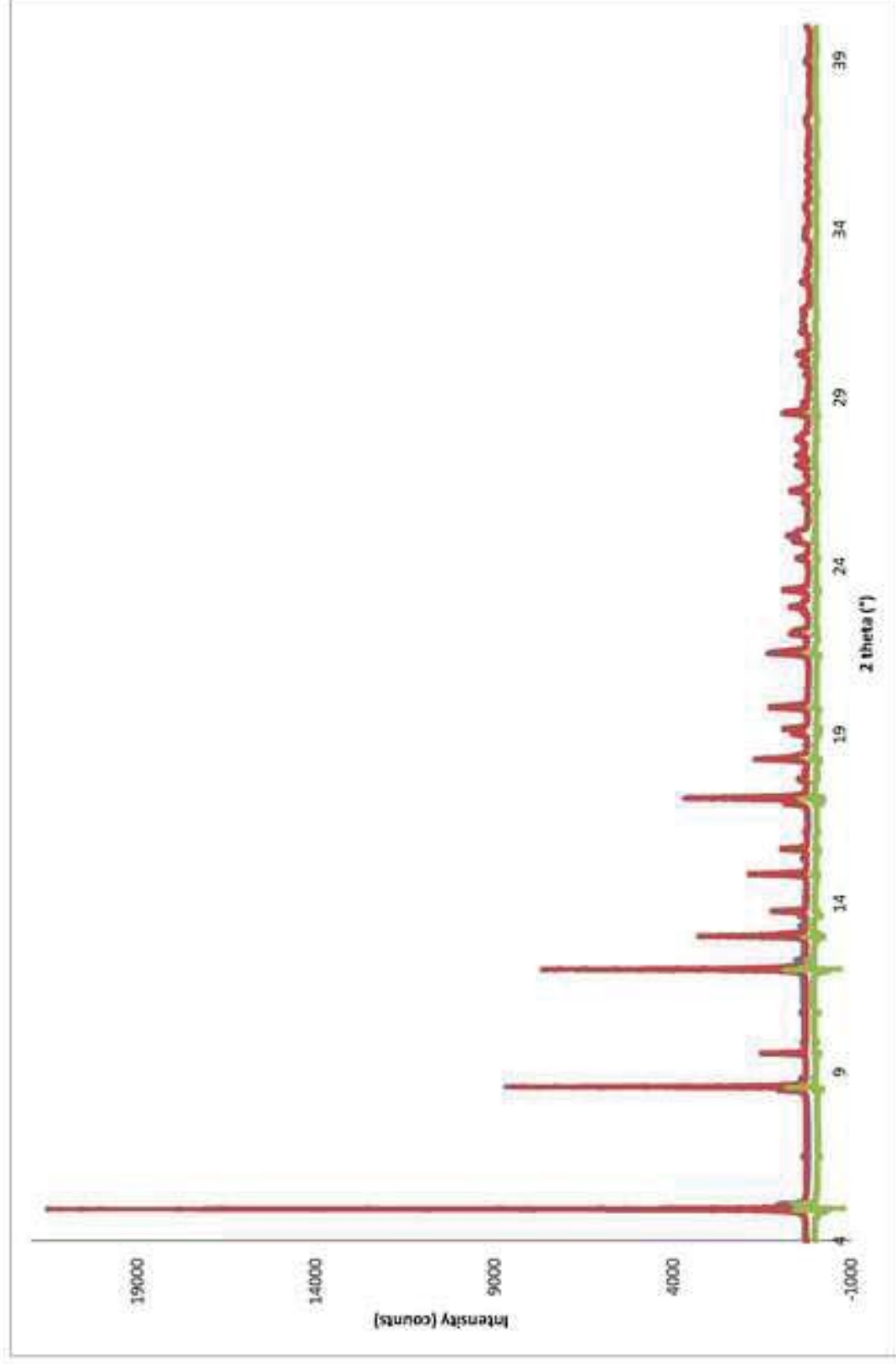


Fig ESI5.jpg
[Click here to download high resolution image](#)



Highlights

- A new ettringite-type phase, $\text{Ca}_6[\text{Ga}(\text{OH})_6 \cdot 12\text{H}_2\text{O}]_2(\text{SO}_4)_3 \cdot 2\text{H}_2\text{O}$ is reported.
- Two new thaumasite phases, $\text{Ca}_6[\text{M}(\text{OH})_6 \cdot 12\text{H}_2\text{O}]_2(\text{SO}_4)_2(\text{CO}_3)_2$, $\text{M} = \text{Mn}, \text{Sn}$ are reported.
- We highlight the preference of tetravalent cations to form thaumasite-type phases.